

***C9orf72* repeat expansion creates the unstable folate-sensitive fragile site FRA9A**

Mila Mirceta^{1,2}, Monika H.M. Schmidt^{1,2}, Natalie Shum^{1,2}, Tanya K. Prasolava¹, Bryanna Meikle^{1,2}, Stella Lanni¹, Mohiuddin Mohiuddin¹, Paul M. McKeever³, Ming Zhang^{3,4,5,6}, Minggao Liang^{1,2}, Ilse van der Werf⁷, Stefaan Scheers⁷, Patrick A. Dion^{8,9}, Peixiang Wang¹, Michael D. Wilson^{1,2}, Theresa Abell¹⁰, Elliot A. Philips¹⁰, Łukasz J. Sznajder^{11,12}, Maurice S. Swanson¹¹, Mustafa Mehkary^{1,2}, Mahreen Khan^{1,2}, Katsuyuki Yokoi¹, Christine Jung¹³, Pieter J. de Jong¹³, Catherine H. Freudenreich¹⁰, Philip McGoldrick³, Ryan K.C. Yuen^{1,2}, Agessandro Abrahão¹⁴, Julia Keith¹⁴, Lorne Zinman¹⁴, Janice Robertson³, Ekaterina Rogueva³, Guy A. Rouleau^{8,9,15}, R. Frank Kooy⁷ and Christopher E. Pearson^{1,2,*}

¹Program of Genetics and Genome Biology, Peter Gilgan Centre for Research and Learning, The Hospital for Sick Children, 686 Bay Street, Toronto, M5G 0A4, Canada

²Department of Molecular Genetics, University of Toronto, 1 King's College Circle, Toronto, ON, M3S 1A8, Canada

³Tanz Centre for Research of Neurodegenerative Diseases, University of Toronto, 60 Leonard Avenue, Toronto, M5T 2S8, Canada

⁴The First Rehabilitation Hospital of Shanghai, Department of Medical Genetics, School of Medicine, Tongji University, Shanghai, 200090, China

⁵State Key Laboratory of Cardiology and Medical Innovation Center, Shanghai East Hospital, School of Medicine, Tongji University, Shanghai, China

⁶Advanced Study, Tongji University, Shanghai, 200092, China

⁷Department of Medical Genetics, University of Antwerp, Belgium

⁸Montreal Neurological Institute-Hospital, McGill University, 3801 University Avenue, Montreal, Quebec, H3A 2B4, Canada

⁹Department of Neurology and Neurosurgery, McGill University, 3801 University Avenue, Montreal, Quebec, H3A 2B4, Canada

¹⁰Department of Biology, Tufts University, 200 Boston Avenue, Medford, MA 02155, USA

¹¹Department of Molecular Genetics and Microbiology, Center for NeuroGenetics and the Genetics Institute, College of Medicine, University of Florida, 2033 Mowry Road, Gainesville, FL 32610-3610, USA

¹²Department of Chemistry and Biochemistry, University of Nevada, 4003-4505 South Maryland Parkway, Las Vegas, NV 89154, USA

¹³BACPAC Resource Center, Children's Hospital Oakland Research Institute, 25129 NE 42nd Pl, Redmond, WA 98053, USA

¹⁴Sunnybrook Health Sciences Centre, 2075 Bayview Avenue, North York, Toronto, ON, M4N 3M5, Canada

¹⁵Department of Human Genetics, McGill University, 3801 University Avenue, Montreal, Quebec, H3A 2B4, Canada

*To whom correspondence should be addressed. Tel: +1 647 388 5151; Email: cepearson.sickkids@gmail.com

Abstract

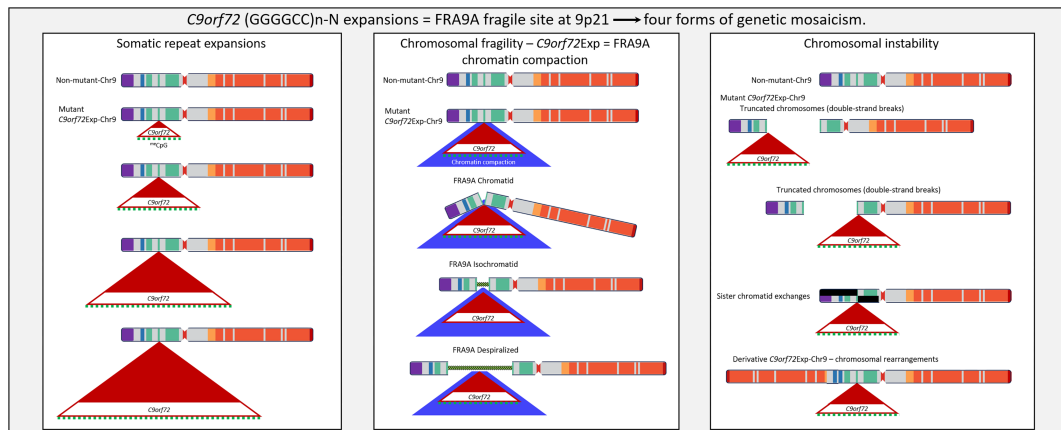
The hyper-unstable Chr9p21 locus, harbouring the interferon gene cluster, oncogenes and *C9orf72*, is linked to multiple diseases. *C9orf72* (GGGGCC)_n expansions (*C9orf72*Exp) are associated with incompletely penetrant amyotrophic lateral sclerosis, frontotemporal dementia and autoimmune disorders. *C9orf72*Exp patients display hyperactive cGAS-STING-linked interferon immune and DNA damage responses, but the source of immunostimulatory or damaged DNA is unknown. Here, we show *C9orf72*Exp in pre-symptomatic and amyotrophic lateral sclerosis-frontotemporal dementia patient cells and brains cause the folate-sensitive chromosomal fragile site, FRA9A. FRA9A centers on >33 kb of *C9orf72* as highly compacted chromatin embedded in an 8.2 Mb fragility zone spanning 9p21, encompassing 46 genes, making FRA9A one of the largest fragile sites. *C9orf72*Exp cells show chromosomal instability, heightened global- and Chr9p-enriched sister-chromatid exchanges, truncated-Chr9s, acentric-Chr9s and Chr9-containing micronuclei, providing endogenous sources of damaged and immunostimulatory DNA. Cells from one *C9orf72*Exp patient contained a highly rearranged FRA9A-expressing Chr9 with Chr9-wide dysregulated gene expression. Somatic *C9orf72*Exp repeat instability and chromosomal fragility are sensitive to folate deficiency. Age-dependent repeat instability, chromosomal fragility and chromosomal instability can be transferred to CNS and peripheral tissues of transgenic *C9orf72*Exp mice, implicating *C9orf72*Exp as the source. Our results highlight unappreciated effects of *C9orf72* expansions that trigger vitamin-sensitive chromosome fragility, adding structural variations to the disease-enriched 9p21 locus, and likely elsewhere.

Received: November 4, 2024. Editorial Decision: November 5, 2024. Accepted: November 11, 2024

© The Author(s) 2024. Published by Oxford University Press on behalf of NAR Molecular Medicine.

This is an Open Access article distributed under the terms of the Creative Commons Attribution License (<https://creativecommons.org/licenses/by/4.0/>), which permits unrestricted reuse, distribution, and reproduction in any medium, provided the original work is properly cited.

Graphical abstract



Introduction

Expansions of 30–7950 GGGGCC repeats in the *C9orf72* gene, which resides in 9p21 (*C9orf72Exp*), are the most common cause of amyotrophic lateral sclerosis (ALS), frontotemporal dementia (FTD) and numerous seemingly unrelated diseases including inflammation dysregulation, autoimmune diseases, over-expression of type I *IFN* genes (1–6) and melanoma (7). Most *C9orf72Exp* carriers are asymptomatic at 40 years of age, some will develop ALS, FTD, another co-occurring disease, or a mixture of these, while many can be disease-free into their 80s and 90s (8,9). This incomplete penetrance and clinical diversity suggest the involvement of genetic and environmental modifiers and/or cumulative events.

Many studies on *C9orf72Exp* disease have focused on the expanded repeat RNA and Repeat-Associated Non-AUG RAN-peptides, where many model systems are devoid of the endogenous chromosomal expanded repeat. Repeat expansions downregulate *C9orf72Exp* expression leading to reduced C9ORF72 protein levels (10,11). Stimulator of Interferon Genes (STING), which with cyclic GMP-AMP synthase (cGAS) activates the innate immune response following sensing of cytosolic double-stranded DNA that could arise from viruses, damaged mitochondria or damaged chromosomes leaked from micronuclei (MN). In *C9orf72Exp* individuals, decreased C9ORF72 leads to STING-hyperactivated *IFN* expression and inflammation in vulnerable neurons (12), but the source of the immunostimulatory DNA is unknown (4,13,14). Accumulating evidence supports the role of an activated DNA damage response (DDR) in *C9orf72Exp* disease (15–25), yet the source of the damaged DNA is unknown. Massive post-natal inter- and intra-tissue repeat length instability is evident in post-mortem tissues of *C9orf72Exp* individuals with the largest somatic expansions in the brain (26–30). Surprisingly, there have been no prior cytogenetic or chromosomal instability studies of *C9orf72Exp*. The recent discontinued clinical programs of antisense oligonucleotides targeting the sense-strand *C9orf72* mRNA, which successfully reduced the RAN-peptides, but resulted in no clinical benefit or trended toward greater clinical decline for the cohort, highlight our poor understanding of *C9orf72Exp* (31–36). A recent meeting focused on the post-trials path forward for *C9orf72Exp* highlighted key areas needing attention: ‘Critical information in our understanding of the biology around the

C9orf72 expansion is still lacking, including what molecular and cellular changes occur at presymptomatic stages...studies of genetics and lifestyles might be useful’ (31). The unknown biology of the *C9orf72Exp* has been highlighted as a focus area (31–36). Factors that may determine disease penetrance, clinical variation, disease onset, progression and severity, are indispensable for family life decisions as well as clinical trial design (6,9,31,37–41).

Genomic context is important, as *C9orf72Exp* occurs on a risk haplotype, which could influence repeat length instability, leading to reduced transcription and its retention of the intron containing the expanded GGGGCC repeat (42–45) (Figure 1). Many of the co-occurring *C9orf72Exp* symptoms can arise independent of a *C9orf72Exp* and are associated with other 9p21 genes. For example, the type I interferon (*IFN*) cluster of 17 genes, including *IFNk* adjacent to *C9orf72*, are linked to autoimmune diseases (e.g. dysregulated inflammation, lupus, rheumatoid arthritis, diabetes and multiple sclerosis) (1,3–5,7). The enhancer-rich 9p21 gene desert is associated with *IFN* signaling (46,47). *CDKN2A/B*, *EMICER1* and *IFNs* are linked to melanoma (48), a cancer recently associated with *C9orf72Exp* (7). *LINGO2*, *TOPORS*, *APTX* and *DNAJA1* have been associated with neurodevelopmental, neurodegenerative and motoneuron disease (49).

The 9p21 locus is hyper-prone to various recurrent structural rearrangements (50–54) (Figure 1). 9p deletion/duplication syndrome includes 9p21.2 as a breakpoint hotspot (55,56). Instability in cancers is suspected to involve chromosomal fragile sites although the hyper-unstable 9p21 has no molecularly mapped fragile site (57). ‘Rare’ fragile sites can be present in as few as a single individual, as initially reported for FRA9A (58), to $\leq 5\%$ of individuals and are linked to partially penetrant neurological disorders, as reviewed (59). Most rare fragile sites are folate-sensitive fragile sites (FSFS), induced in the absence of folate or by the antimetabolite 5-fluorodeoxyuridine (FUdR). Ten of the ~ 30 FSFS have been mapped to gene-specific expanded (CGG) $_n$ repeats, including FRA9A, FRA9B, FRA9C, FRA9D, FRA9E, FRA9F, FRA9G, FRA9H, FRA9I, FRA9J, FRA9K, FRA9L, FRA9M, FRA9N, FRA9O, FRA9P, FRA9Q, FRA9R, FRA9S, FRA9T, FRA9U, FRA9V, FRA9W, FRA9X, FRA9Y, FRA9Z and FRA9AA. FSFS are prone to DNA breaks making them mutation hotspots—mutations that can alter clinical presentation, which is well-characterized for the CGG-expanded FRA9A/*FMR1*, reviewed in (59). Through >75 years of study, many isolated case reports, diverse mutation forms

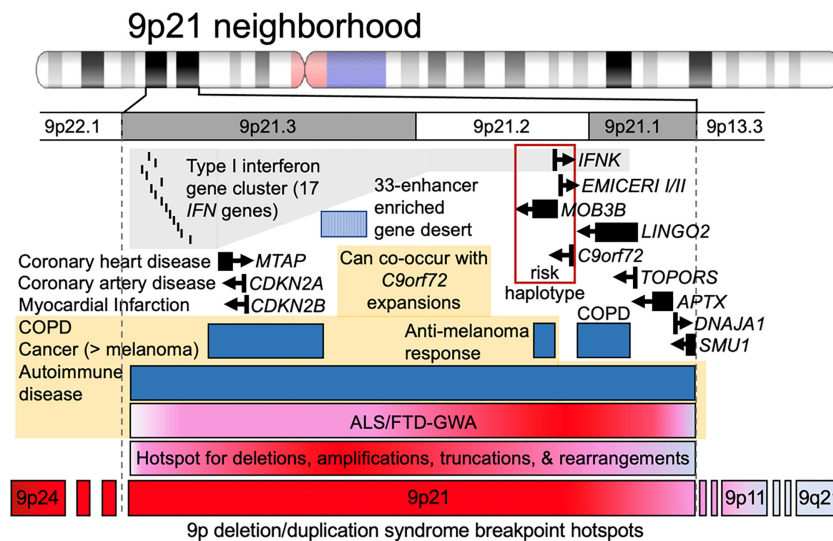


Figure 1. The 9p21 neighborhood, associated genes, diseases and instability hotspots. See the text.

(varying CGG expansion sizes, contiguous gene deletions, gene duplications, intra- and inter-chromosomal recombination and point mutations), and *FMR1* mosaic epimutations have been identified as the cause of numerous seemingly unrelated diseases, many incompletely penetrant (59). Individual case studies with deep clinical, neuropathological and molecular phenotyping can be informative of disease etiology. Thus, the instability of FSFS can impact disease manifestation and clinical presentation. Our objective was to better understand the biology of the endogenous expanded *C9orf72* repeat in the context of 9p21 in presymptomatic and disease states. We assessed whether the expanded *C9orf72* repeat, GGGGCCGGGGCCGGGGCCGGGGCC..., which contains the CGG-motif common to all mapped FSFS, is a FSFS.

Materials and methods

In silico datasets and analyses

Sequence feature and epigenetic datasets used in Figure 2 and Supplementary Figure S1 are described as follows. Repeat annotations and %GC tracks were obtained from the UCSC genome browser (hg19). Wavelet-summarized replisq data (ENCODE) was obtained in bigWig format from GEO:GSE34399. Erythroblast SNS-seq data and replication origins were obtained in bedGraph and bed format, respectively, from GEO:GSE6197. Imputed %DNA methylation for GM12878 was obtained from the roadmap epigenomics data portal (<https://egg2.wustl.edu/roadmap/data/byFileType/signal/consolidatedImputed/DNAMethylSBS/E116-DNAMethylSBS.imputed.FractionalMethylation.signal.bigwig>). Pre-calculated second-order DNA shape features were obtained from the Rohs lab GBSshape database.

Cell culture and fragile site induction

All cytogenetic studies were performed using Epstein-Barr virus-transformed lymphoblastoid cell lines from *C9orf72*-ALS patients, expansion carriers and control individuals provided by Dr Guy Rouleau (McGill University). One of the patients, P4, displayed signs of FTD. All patients provided written informed consent. Cells were cultured in RPMI 1640

media supplemented with 15% fetal bovine serum (FBS) (ThermoFisher Scientific), 2 mM L-glutamine, Pen/Strep (100 IU/ml, 100 µg/ml) and 1 mM sodium pyruvate. Two modes of FSFS induction were used to demonstrate fragility at 9p21.2: (i) 24 h with 0.1 µM FUDR (an anti-folate) or (ii) 14 days with low-folate Media 199 (Gibco, Cat #: 11150-059) supplemented with 2% fetal calf serum (FCS), 2 mM L-glutamine and Pen/Strep (100 IU/ml, 100 µg/ml). Cells in 199 media were treated with 100 nM methotrexate for 16 h, washed and then treated with 0.01 µM bromodeoxyuridine (BrdU) for a total of 3 h prior to harvest. All cells were treated with 6 µg/ml ethidium bromide (EtBr) and 0.05 µg/ml KaryoMAX (Gibco; Cat #: 15 212 012) prior to harvest. Cells were then centrifuged and resuspended in 0.075 M KCl solution for 30 min at 37°C followed by several washes with fixative solution (3:1 methanol:acetic acid). Long-term FUDR culture experiments were performed in either RPMI 1640 media (as described above) or Roswell Park Memorial Institute Medium (RPMI) 1640 media + 0.1 µM FUDR for a total of 8 weeks. Media and FUDR were replaced every 2–3 days. Cells were harvested at 1-, 2-, 4-, 6- and 8-week time points for DNA purification, and Southern blot was run as described below.

Metaphase chromosome and FISH analysis

Slide preparations for both cytogenetic and fluorescent *in situ* hybridization (FISH) analysis of metaphase spreads were made from fixed cell suspensions using a Model CDS 5 Cytogenetic Drying chamber according to standard methods. For 199 media conditions, breaks and gaps were quantified on total Giemsa stained metaphases and subsequently G-banded to karyotype each metaphase and confirm fragile site on 9p-arm. SpectrumGreen and SpectrumOrange-conjugated dUTP probes (RP11-15P13, RP11-274I21, RP11-1149M23, RP11-491J7, RP11-945G22, RP11-1079P2, RP11-360B21 and RP11-696J10) from RPCI-11 human BAC library were generated by The Centre for Applied Genomics (TCAG, PGCL, Toronto, Canada) using the Vysis nick translation kit (Cat #07J00-001; Abbott Molecular, Illinois, USA) in accordance with manufacturer's instructions. Chromosomes were counterstained with 4',6-diamidino-2-phenylindole (DAPI). One hundred metaphases per sample were scored for each

condition using either brightfield microscopy, Olympus IX81 quorum spinning disk confocal microscope or Zeiss Axio-plan 2 fluorescence microscope. Images were collected using a CCD camera (Hamamatsu C9100-13 EM-CCD, Hamamatsu, Japan) (Princeton Instruments Pentamax, Roper Scientific, New Jersey, USA) and analyzed using Volocity (Perkin Elmer, Massachusetts, USA) or CytoVision (Leica Biosystems, Germany) software.

Southern blot analysis of *C9orf72* repeat expansion size

Southern blot analysis was performed to size *C9orf72* repeat expansions as this method is the gold standard for sizing large (GGGGCC)_n repeat expansions (28). Southern blotting provides an estimate of non-bias expansion sizes (60). We used the Southern blotting method (28,61) with 241 bp probe, which anneals 153 bp upstream of the (GGGGCC)_n repeat tract, and used selected restriction-endonuclease digestions of genomic DNA (as noted in the figures), which permit sensitive detection of repeat size and length heterogeneity at molar levels. The 241 bp probe was produced by polymerase chain reaction (PCR) using primers (Fwd: 5'-AGAACAGGACAAGTTGCCCC-3' and Rev: 5'-AACACACACCTCCTAAACCC-3') as published (28,61). For mapping boundaries of MNase accessibility an additional probe was used (see below). Molecular weight markers were used to estimate the size of repeats. Distances between molecular weight markers were measured using ImageLab software (BioRad) and plotted against the known number of base pairs for each marker. A best-fit linear regression was calculated in Microsoft Excel and the equation of this line was used to calculate the size of each band on the blot. Different restriction enzyme combinations were used to cut the genomic DNA, as noted in each figure, hence resulting in different flank repeat sizes.

Methylation analysis of the *C9orf72* repeat

Methylation analyses were done in blinded experiments using the same DNA prep as for Southern blot. Genomic DNA was bisulfite converted using the EZ DNA Methylation-Lightning™ Kit (Zymo). We estimated the number of methylated CpG-sites at the CpG-island 5' of the (GGGGCC)_n repeat using bisulfite sequencing as reported previously (62). To estimate the methylation of the (GGGGCC)_n repeat itself, we used a qualitative GGGGCC-methylation assay, sensitive enough to detect repeat methylation in a mixture containing ~5% high-methylated DNA standard (63). We always observed methylation mosaicism for expanded repeat samples, revealed by the presence of the amplification product of the expansion in both methylated (blue) and unmethylated (green) channels (64).

Micronucleus and nuclear bud detection

MN and nuclear bud (NBud) analyses were done as previously described with some modifications (65–67). Briefly, cells were treated with 0.5 μM FUDR for a total of 24 h, with cytochalasin B (4 μg/ml) being added 3 h after addition of FUDR. Cells were briefly incubated in 0.075 M KCl, fixed with Carnoy's fixative and slides with sparsely spread cells were prepared using a Model CDS 5 Cytogenetic Drying chamber (Thermotron, Michigan, USA). Spectrum-Green (RP11-696J10) and SpectrumOrange (RP11-672M4)-

conjugated dUTP probes from RPCI-11 human BAC library were generated by The Centre for Applied Genomics (TCAG, PGCRL, Toronto, Canada) using the Vysis nick translation kit (Cat #07J00-001; Abbott Molecular, Illinois, USA) in accordance with manufacturer's instructions. Nuclei were counterstained with DAPI. At least 950 binucleated cells were scored per condition for the presence of MN and NBuds and Chr9 signals, as previously described (66). Two blinded and independent experiments were carried out for each data asset. Statistical analyses were done using Fisher's exact test for the combined values of MN and NBud events as they are believed to arise from the same phenomenon (66,68). Images were captured using an Olympus BX61 fluorescence microscope. Images were collected using a CCD camera (Hamamatsu C9100-13 EM-CCD, Hamamatsu, Japan) (Princeton Instruments Pentamax, Roper Scientific, New Jersey, USA) and analyzed using ASI SpotScan software (Applied Spectral Imaging, California, USA).

Sister-chromatid exchange (SCE) assay

Cells were incubated in the presence of 10 μM BrdU for two cell cycle periods and pulsed with 0.1 μg/ml of KaryoMAX (Gibco; Cat #: 15 212 012) for the last 2 h before being harvested. FUDR (0.1 μM) was added for the last cell cycle. Harvested cells were treated with 0.075 M KCl for 20 min and subsequently fixed with methanol:acetic acid (3:1) for at least 30 min. Cells were fixed onto glass slides. Dried slides were incubated with 10 μg of Hoechst 33 258 per ml in phosphate buffer (pH 6.8) for 20 min, followed by rinsing with MacIlvaine solution (164 mM Na₂HPO₄, 16 mM citric acid [pH 7.0]). Slides were irradiated with UV light for 2 h and incubated in 2X SSC solution at 62°C for 1 h before staining with 5% Giemsa solution and subsequent microscopy. At least 100 metaphase cells were evaluated for sister-chromatid exchange (SCE) events genome-wide per genotype. For Chr9-specific SCEs, slides were destained with xylene solution followed by methanol:acetic acid (3:1) and then standard FISH procedures, as described above were followed using SpectrumOrange-dUTP conjugated RP11-696J10 probe. At least 30 of the same Giemsa-stained metaphases were relocalized using fluorescence microscopy and imaged to allow for quantification of SCEs specifically on the 9p- and 9q-arms.

Construction of plasmids and yeast strains

An XbaI-HindIII fragment containing a region of the human *C9orf72* gene with an expanded (GGGGCC)_n repeat and 547 bp of flanking sequence (from pcDNA3.1 (+)c9-200 + obtained from R.H. Brown; CF stock #435) was cloned into the MCS of plasmid pEP1 to create plasmids pEP1-(GGGGCC)_n. pEP1 was made by cloning the *ADE2* gene from pRS402 into the BsaAI and NsiI sites of pHZ1; pHZ1 was made by cloning the G4T4 sequence into the SmaI site of pYIP5. The CAG repeat was cloned into pEP1 XhoI and XbaI sites. Repeat lengths in plasmid clones were confirmed by sequencing. Repeat lengths of the (GGGGCC)_n plasmids were ~16, 29 and 36 for plasmids 504, 484 and 485, respectively; the exact number of repeats varied with different sequencing runs. Plasmids were linearized with XcmI and recombined into the *URA3* marked yeast artificial chromosome (YAC) CF1 in strain VPS105 (CFY #289) to create the new GGGGCC-*ADE2*-*URA3* and CAG-*ADE2*-*URA3* YACs (see Supplementary Figure S7A and D), which were confirmed for

YAC structure by PCR. CAG tract lengths were confirmed by sequencing of PCR amplicons but (GGGGCC)_n tract lengths could only be determined approximately by Southern blot since amplification from genomic DNA was unsuccessful, and are therefore reported to the nearest 5 bp.

YAC fragility assay

End loss of the repeat-*ADE2-URA3* YACs was determined by an established protocol (69) except that 1 ml of an overnight culture inoculated with a specific colony was plated on media containing 5-Fluoro-Orotic Acid (FOA) and a low amount of adenine but lacking leucine (FOA-Leu low Ade) to determine the number of mutants, and a dilution was plated on yeast complete media lacking leucine (YC-Leu) for a total cell count. Rates were determined by the method of the median. Another 1 ml of the same culture was used to isolate genomic DNA for Southern blot to assess repeat length. For reasons not completely understood, but that could include reduction of transcription through the repeat tract, the insertion of the *ADE2* marker resulted in a lower rate of FOA^R compared to previously published values for the CAG-85 YAC without the *ADE2* gene. End loss was confirmed in a subset of colonies (usually one from each FOA-Leu plate) by PCR (retention of the sequence to the left of the G₄T₄ telomere seed and loss of sequence to the right of the repeat tract; [Supplementary Figure S7](#)).

Southern blot—yeast

Yeast genomic DNA was digested with NheI and XbaI restriction enzymes, separated by horizontal gel electrophoresis and blotted to a nylon membrane using a standard Southern protocol. Either the Roche Molecular Weight Marker VI or VII was run as a size marker. For the preparation of the probe, a 301 bp fragment adjacent to the (GGGGCC)_n repeat was PCR amplified from DNA of plasmid #485 as a template, using Primers #1402 (ALSsouthernFOR) and #1403 (ALSsouthernREV). Probes were labeled using the DIG High-Prime DNA Labeling and Detection Starter Kit I (Cat #: 11 745 832 910; Roche). Repeat tract estimation was performed as previously described (Southern blot analysis of repeat expansion size).

Chromatin accessibility *in cellulo* with MNase

Human lymphoblast cell lines from *C9orf72*-expansion carriers were assessed for MNase accessibility, as outlined in [Figure 5B](#). Briefly, cell pellets were washed in ice-cold 1X PBS, re-pelleted and permeabilized by ice-cold NP-40 lysis buffer (10 mM Tris pH 7.4, 10 mM NaCl, 3 mM MgCl₂, 0.5% NP-40, 0.15 mM spermine, 0.5 mM spermidine) for 5 min on ice. Nuclei were collected at 200 × *g* (10 min, 4°C), washed in 1X MNase digestion buffer (10X stock: 100 mM Tris pH 7.4, 150 mM NaCl, 600 mM KCl, 5 mM spermidine, 1.5 mM spermine), re-pelleted and subsequently resuspended in 1X MNase digestion buffer supplemented with 1 mM CaCl₂. Treatment followed with MNase for 5 min at 22°C, at differing concentrations (refer to [Figure 5](#) and [Supplementary Figure S4A](#)—all serial dilutions). All digestion reactions were stopped with an equal volume of *Stop* solution (0.625 mg/ml proteinase K, 20 mM EDTA (ethylene glycol-bis(β-aminoethyl ether)-N,N,N',N'-tetraacetic acid), also known as egtazic acid), 20 mM EGTA, 1% SDS diluted in 1X MNase buffer) and incubated at 37°C for a minimum of 1 h. Reaction conditions were optimized to ensure over-digestion by MNase, which

diminishes MNase cleavage preference. DNA was purified by phenol/chloroform extraction, RNase A treatment and ethanol precipitation. A small amount of purified DNA was assessed for completeness of MNase digestion, by its conversion to mono-, di- and tri-nucleosome sized fragments as resolved by electrophoresis stained with EtBr and visualized by UV imaging ([Figure 5B](#), left panel; [Supplementary Figure S4A](#)). DNA samples were analyzed by Southern blot as described.

Chromatin accessibility in post-mortem tissues with MNase

We conducted MNase accessibility analysis using post-mortem brain tissues (orbito-frontal cortex and cerebellum) of an asymptomatic 90-year-old male and his 59-year-old ALS-FTD-affected daughter, previously deep-phenotyped (summarized in [Supplementary Table S2](#)) (29,70). The asymptomatic male carried 70-repeat *C9orf72* expansion in the blood and was deceased at 90 years of age. Tissue was Dounce homogenized using 1X MNase digestion buffer, 10% NP-40 was added to final concentration 0.5%, incubated 5 min on ice, filtered through a 40 μm strainer and centrifuged. Nuclei pellets were washed in MNase digestion buffer and incubated with different concentrations of MNase. Remaining steps were performed as described above.

Digestibility of *C9orf72* BAC DNA *in vitro* with MNase

A bacterial artificial chromosome (BAC) containing ~160 (GGGGCC)_n(GGCCCC) repeats, prepared in the lab of Piet de Jong, was restricted by NheI and XhoI giving rise to a shorter fragment of ~1750 base pairs, which was gel-purified. Half (by volume) of the purified product underwent CpG-methylation by M.SssI methyltransferase supplemented with 640 μM S-adenosylmethionine (New England Biolabs) and purified using the QIAEX II kit (Qiagen). Completeness of methylation was checked by the inability to be digested by the methyl-sensitive HpaII but successful digestion by the methyl-insensitive *MspI*. Subsequently, in parallel, equal concentrations (~100 ng/reaction) of the non-methylated and methylated fragments were treated with increasing levels of MNase (0U–0.1U–1U–5U–25 U) for 5 min at 22°C in 1X MNase digestion buffer. The MNase reaction was halted by addition of 6X purple loading dye (New England Biolabs) and electrophoresed immediately on a 1% agarose gel at 50 V for 20 min, followed by 100 V for 100 min. Gene Ruler Mix (Thermo Scientific) was loaded in the first lane. Electrophoresed products were stained with EtBr, visualized by UV imaging ([Supplementary Figure S4B](#), left hand side), and DNA fragments were transferred to a positively charged nylon membrane, and probed with a 177 bp probe, annealing just upstream of the GGGGCC repeat tract ([Supplementary Table S1](#)). To maximize our ability to assess that loss of signal corresponded to MNase digestion of the GGGGCC repeat fragment, we developed the 177 bp probe which anneals immediately adjacent to the repeat. The 177 bp probe anneals 7 bp upstream of the GGGGCC repeat tract, while the 241 bp probe anneals 153 bp upstream. The 177 bp probe was produced by PCR using primers (Fwd: 5'-GAGCAGGTGTGGGTTTAGGA-3' and Rev: 5'-CGACTCCTGAGTTCAGAGC-3') ([Supplementary Table S1](#)). A phosphor image of the Southern blot was obtained

using the Typhoon system (Supplementary Figure S4B, right hand side), and the rate of digestion of probed sequence was calculated using densitometric analysis in ImageJ. The percentage of DNA resistant to MNase (therefore, the fraction of undigested 'starting fragment' BAC DNA) was plotted as a function of MNase units of activity (concentration) in Graph-Pad Prism 8 (Supplementary Figure S4B).

MNase controls

The MNase resistance we observe is not a reflection of the sequence preference of MNase or the sequence composition of the *C9orf72* region. The MNase resistance spanning the mutant *C9orf72* locus supports altered chromatin packaging of the non-repetitive flanks, as the 241 bp probe anneals 153 bp upstream of the (GGGCC)_n repeat, and resistance is still evident (Figure 5). The relative resistance of the expanded allele compared to the internal control of the non-mutant *C9orf72* allele, provides strong support for altered chromatin accessibility. MNase is known to display a cleavage sequence preference, preferring 5'-NpT and 5'-NpA sites (71,72), yet is capable of digesting G-C only sequences and can digest most calf thymus DNA with over-digestion, which diminishes MNase cleavage preference (71). All of our nuclear digests were completed to over-digestion. The *C9orf72* sequences flanking the repeat, that are probed herein, contain an extensive number of the preferred 5'-NpT and 5'-NpA sites (Supplementary Figure S2B, green font). That protein-free genomic DNA from *C9orf72* expansion carriers is digested at an equal rate relative to the internal equimolar control of the non-expanded *C9orf72* allele, supports that the flanks can be digested (Supplementary Figure S4A). The MNase digest of the purified (GGGGCC)₁₆₀ repeat DNA further confirms that the pure GC-rich repeat can be digested by MNase as evidenced by the EtBr-stained gel (Supplementary Figure S4B). As such, the reduced digestion of the expanded allele in its native chromatinized state represents a chromatin-mediated inaccessibility.

To rule out possible artefacts such as differences in the sensitivity between EtBr staining and Southern probe hybridization, or loss of DNA during Southern transfer, or an uneven transfer or membrane retention of DNA, an aliquot of the same samples was run on a high-resolution gel, ethidium-stained, hybridized with the *C9orf72*-specific probe, imaged, and then the blot was stripped and re-probed using radiolabeled total genomic DNA as the probe (Supplementary Figure S4A). The hybridization pattern from total genomic DNA probe is very similar to the EtBr-stained gel: most of the genome has been digested to completion to mono-, di-, tri- and tetra-nucleosome sized fragments (Supplementary Figure S7A). In contrast, hybridization with the *C9orf72* probe shows dramatic MNase resistance of the expanded allele, while the non-expanded allele appears to be digested at the same rate as the rest of the genome.

Control MNase digestions of protein-free genomic DNA of unmethylated and methylated *C9orf72*-ALS samples, compared to the chromatinized samples of the same cell lines showed that MNase digestion occurs similarly for both alleles at extremely low MNase concentrations (0.01 Units) in protein-free conditions, yet the expanded allele is strongly resistant in chromatinized samples, supporting that this resistance is due to an unusual chromatin state (Supplementary Figure S4B and C).

There is a striking difference in MNase digestion between the ethidium-stained bulk genomic DNA, and the Southern blot detected *C9orf72* expanded allele, which is internally controlled for by its non-expanded homolog (Figure 5). See above notes and Supplementary Figure S4 for controls. The *C9orf72* region showed reduced presence in the mono-, di- and tri-nucleosomal digested regions, relative to the rest of the genome (compare Southern blot with ethidium stain, Figure 4A).

Control MNase digests using cloned *C9orf72* expanded (GGGGCC)₁₆₀ repeat and flanks (\pm CpG-methylation) were performed to assess the impact of MNase sequence selectivity and the influence of CpG-methylation on digestibility. As shown in Supplementary Figure S4B, the expanded repeat itself can be completely digested by MNase, and under the conditions used, the effect of sequence and CpG-methylation had limited effects on MNase digestibility, as previously reported (71,72). This is consistent with the extensive number of the MNase-preferred 5'-NpT and 5'-NpA sites (71,72) in the *C9orf72* sequences flanking the repeat that are probed in the Southern blot (Supplementary Figure S2B, green font). These controls, coupled with the equal rate of MNase digestion of the protein-free *C9orf72* expanded allele in genomic DNA relative to the internal control of the non-expanded *C9orf72* allele (Supplementary Figure S4A,ii), demonstrate that the expanded repeat and flanks can be digested by MNase. Thus, the inaccessibility of MNase to the chromatinized *C9orf72* expanded allele and flanks (where the Southern probe binds) is due to its unusual chromatin compaction, and is not due to an inherent inability of MNase to cleave the expanded (GGGGCC)_n DNA sequence.

Further mapping of the MNase accessibility in the chromatinized *C9orf72* expanded cells, with and without aberrant methylation, was performed. Essentially, for large expansions the mutant *C9orf72* allele is less accessible to MNase ~3300 bp upstream and ~2500 bp downstream of the expanded repeat. Decreased accessibility is further exacerbated by aberrant methylation (detailed in Supplementary Figure SD4A,iii). The absolute boundaries of decreased MNase accessibility varied with repeat expansions.

Mapping MNase accessibility boundaries

We mapped the boundaries of MNase resistance in patient cell lines with no expansions (WT), expansions (P1 and P7) and expansions with methylation (P3 and P6), using a series of post-MNase restriction digests upstream and downstream of the repeat; fragments were detected by Southern blotting using either the 241 or 177 bp probe, as indicated. Upstream mapping was carried out with a post-MNase genomic digestion using BanI, which cleaves just downstream of the repeat, in combination with either one of a series of restriction digests progressing along the upstream flank, as far as 3335 bp upstream (AflII, EcoRI, PvuII and SphI) (Supplementary Figure S4C). These samples were assessed by Southern blot, detected with the 177 bp probe (Supplementary Figure S4C upper panel, schematic). For each restriction fragment, the non-expanded allele signal was completely lost while the expanded allele was either resistant or partially digested to a shorter, distinct, nearly repeat-only containing fragment. This might suggest that the repeat tract itself is the most resistant to MNase accessibility. The amount of MNase-resistant starting material decreases progressively with increasing distance upstream from

the repeat (Supplementary Figure S4C). Thus, the MNase resistance of the mutant allele extends upstream of the repeat at least ~1252 bp to the PvuII site, where some of the full-length fragment is still inaccessible to MNase, but diminishes further upstream ~3335 bp to the SphI site (Supplementary Figure S4C). Downstream mapping was conducted using a post-MNase genomic digestion with AflIII, which cleaves upstream of the repeat and beside the region detected by the 241 bp probe. AflIII digestion was paired with one of a series of restriction digests progressing along the downstream flank, as far as 3750 bp downstream (BanI, BstYI, BamHI, PvuII or PstI) (Supplementary Figure S4C, lower panel, schematic). For each restriction fragment, the expanded allele was resistant and progressively digested to a shorter, distinct nearly repeat-only containing fragment, again suggesting that the repeat tract is the most MNase resistant region. Resistance in the downstream region was more evident for the methylated allele and for larger expansions. For the larger methylated sample, P3 (~3000 repeats), the MNase resistance of the mutant allele extends downstream of the repeat at least ~2440 bp to the PvuII site, where some of the full-length fragment is still inaccessible to MNase, but diminishes further downstream ~3750 bp to the PstI site (Supplementary Figure S4C). For the shorter methylated expansion P6 (~770 repeats), the MNase resistance of the mutant allele extends downstream of the repeat at least ~1714 bp to the BamHI site, where some of the full-length fragment is still inaccessible to MNase, but diminishes further downstream ~3750 bp to the PstI site (Supplementary Figure S4C). Thus, the MNase resistance of the mutant allele extends at least ~2440 bp downstream from the repeat to the PvuII site, where some of the full-length starting fragment is still resistant downstream ~3750 bp to the distal PstI site (Supplementary Figure S4C). The methylated and expanded allele was more resistant than the non-methylated expanded allele. In summary, for large expansions some of the mutant *C9orf72* alleles can be resistant to MNase ~1250 bp, diminishing through to ~3300 bp upstream and downstream resistance is ~2440 bp, diminishing through to ~3700 bp away from the expanded repeat, and resistance is further exacerbated by aberrant methylation.

Southern blot—*HTT*

Southern blotting for the *HTT* allele was followed as described (73), modifying the probe to be 226 bp, which anneals 143 bp upstream of the (CAG)_n repeat tract, and used selected restriction-endonuclease digestions of genomic DNA—permitting sensitive detection of repeat size and length heterogeneity at molar levels. The 226 bp probe was produced by PCR using primers (Fwd: 5'-CTTGCTGTGTGAGGCAGAAC-3' and Rev: 5'-CGCAGGTTAAAGCAGAACCT-3'). Molecular weight markers were run alongside the DNA (Gene Ruler Mix, Thermo Scientific and Roche Molecular Weight Marker II).

Chromatin accessibility *in cellulo* with MNase

An HD patient fibroblast cell line, with an *HTT* expansion of (CAG)_{21/180} (GM09197) was assessed for MNase accessibility at *HTT*. Cell pellets were washed in ice-cold 1X PBS, re-pelleted and permeabilized by ice-cold NP-40 lysis buffer (10 mM Tris pH 7.4, 10 mM NaCl, 3 mM MgCl₂, 0.5% NP-40, 0.15 mM spermine, 0.5 mM spermidine) for 5 min. on ice. Nuclei were collected at 200 × g (10 min, 4°C), washed in 1X

MNase digestion buffer (10 X stock: 100 mM Tris pH 7.4, 150 mM NaCl, 600 mM KCl, 5 mM spermidine, 1.5 mM spermine), re-pelleted and subsequently resuspended in 1X MNase digestion buffer supplemented with 1 mM CaCl₂. Treatment followed with MNase for 5 min at 22°C, at differing concentrations (0.5–20U). All digestion reactions were stopped with an equal volume of *Stop* solution (0.625 mg/ml proteinase K, 20 mM EDTA, 20 mM EGTA and 1% sodium dodecyl sulfate [SDS] diluted in 1X MNase buffer) and incubated at 37°C for a minimum of 1 h. Reaction conditions were optimized to ensure over-digestion by MNase, which diminishes MNase cleavage preference. DNA was purified by phenol/chloroform extraction, RNase A treatment and ethanol precipitation. A small amount of purified DNA was assessed for completeness of MNase digestion, by its conversion to mono-, di- and tri-nucleosome sized fragments as resolved by electrophoresis stained with EtBr and visualized by UV imaging. Approximately 12 µg of each DNA sample was then restriction digested to completion to release the repeat-containing fragment and flanking regions—this increases resolution by electrophoresis. Following neutral transfer, the *HTT* containing regions were detected by Southern blot as described above.

RNA-seq library preparation, sequencing and analysis

Total RNA from the lymphoblastoid cell lines was isolated using the hot TRIzol extraction protocol (74). Briefly, samples dissolved in TRIzol were incubated in a thermomixer set to 55°C and 1000 rpm for 10 min. After cooling to ambient temperature, RNA was isolated by using TRIzol Reagent and the Direct-zol RNA MiniPrep Kit with DNase treatment according to manufacturer's provided protocol (Zymo Research). RNA was quantitated using Qubit RNA BR Assay Kit (Thermo Fisher Scientific). Strand-specific, rRNA-depleted RNA-seq libraries were prepared using the KAPA Stranded RNA-seq Kit with RiboErase HMR (Kapa Biosystems) per manufacturer's instructions, except for the use of custom Illumina-compatible index primers to allow multiplexing. Library size distribution was assessed using the High Sensitivity NGS Fragment Analysis Kit (DNF-747) on a Fragment Analyzer (Agilent). 2 × 150 paired-end sequencing was performed using an Illumina NextSeq 500. Reads were aligned to the genome assembly GRCh38 (hg38). Salmon was used for transcript expression quantification and differential gene expression analysis was performed using DESeq2 (75,76). A heat map was generated in R using the ggplot2 package. Graph was generated and statistical analysis was performed by using GraphPad Prism 8.

Developing murine tissue-derived cell lines

Mouse tissues for cytogenetic analysis of chromosomes followed published protocols (77–86). Mouse care, sacrifice and tissue harvesting was done on the same day, including three wild-type and three transgenic mice, all 5 months of age. Mice aged 5 months, when cell proliferation in the central nervous system (CNS) and peripheral organs had ceased at 2 months of age (77–79). Ear, lung, tail, cerebrum, cerebellum, brain stem, kidney, liver and spleen were harvested. A section of each tissue was manually macerated then treated with DMEM (Dulbecco's Modified Eagle Medium) + Trypsin-EDTA for 1 h in a 37°C incubator. Cells were collected, spun down and then seeded in a T25 flask with DMEM media supplemented

with 20% FBS and 2 mM L-glutamate. Two flasks were prepared: one with 1% penicillin/streptomycin (Pen/Strep) [100 IU/ml, 100 µg/ml] added and one without. Once confluent, cells were seeded in a new T25 in DMEM (supplemented with 15% fetal bovine serum, Pen/Strep, and 2 mM L-glutamate to begin fragile site induction. To avoid cell type selection and cell type loss due to an inability to adapt to cell culture, harvested tissues were purposely cultured for very short terms following tissue harvesting. When possible, cells were grown to 80% confluency. Avoiding high cell densities, or long periods at confluency, has been shown to diminish FRAXA expression (83). Tissues were harvested and immediately made into cultures. These cultures were grown and induced to express the fragile sites and cytogenetically assessed. There was neither transit delays nor storage of cell lines until fragile sites were induced in metaphase. All procedures, including colony housing and tissue harvesting, were done in-house. Precautions were taken to avoid delays following tissue harvesting, tissue freezing, extended culturing and storage of cells, as these have been noted to diminish fragile site expression (83–86).

Results

9p21 shares sequence and epigenetic features with (CGG)_n FSFS

The *C9orf72* locus and each of the CGG-expanded FSFS share many sequence, structural, functional and epigenetic features (Figure 2A–D and Supplementary Figure S1A–J). Nine of the 10 CGG-FSFS plus *C9orf72* colocalize to boundaries between topologically associating domains and were enriched with CTCF sites and CpG-islands (Figure 2D). Thus, *C9orf72* and CGG-FSFS share with 22 other disease-associated repeat expansion loci these epigenetic features (63). Unlike other disease-associated repeats, both the *C9orf72* GGGGCC and all CGG-FSFS share G4-quadruplex forming repeats (87–89).

Variations in *C9orf72* repeat expansion size, CpG-methylation and disease state permit assessment of contribution to fragility

To study the connection between *C9orf72*Exp and fragility, we characterized lymphoblastoid cells from *C9orf72*Exp families, where some carriers were presymptomatic and some presented with ALS or ALS/FTD (Figure 3A). Sizing *C9orf72* expansions by Southern blots shows repeat length heterogeneity within and between individuals, with expansions ranging from ~300 to ~4400 repeats (Figure 3B and Supplementary Table S1). All individuals carried (GGGGCC)₂ on the non-expanded allele.

Most of our cell lines were CpG methylated in the expanded repeat, with varying levels in flanking CpG-islands, and no methylation in the non-expanded allele (Figure 3B and Supplementary Figure S2), consistent with previous findings of aberrant methylation and levels of methylation mosaicism in *C9orf72*Exp carriers (62,90). We found an absence of methylation, likely arising from methylation mosaicism, in cells of a presymptomatic *C9orf72*Exp (P1) and ALS-affected individuals (P7 and P8). No obvious differences were observed between cells from presymptomatic and affected *C9orf72*Exp individuals. Methylation status was stable, consistent with longitudinally collected samples from *C9orf72*Exp carriers (91). Control cells from individuals without *C9orf72*Exp had no methylation at *C9orf72*. Thus, our *C9orf72*Exp cell line collection permitted assessing fragility in the presence/absence of

methylation and with/without disease of donors (Figure 3A, see right-hand chart).

C9orf72 expansion is the molecular cause of a FSFS at 9p21 (FRA9A)

Fragility was assessed cytogenetically (Figure 4A–D). FUDR-induced fragile sites were observed and localized to 9p21 by FISH, in all eight *C9orf72*Exp cell lines. Fragility was only observed in *C9orf72*Exp cells, with FUDR-treatment and only on one Chr9, consistent with FRA9A (58). Fragility presented in various forms including gaps (isochromatid and chromatid), constrictions and despiralized regions (Figure 4A). Full metaphase spreads and zoomed-in versions, with greater resolution are available upon request. With the exception of the despiralized form, these are similar to forms of FRAXA (59). The despiralized Chr9 was similar to the despiralized heterochromatin in immunodeficiency, centromeric instability and facial anomalies (ICF) syndrome (92). Lengthening of the despiralized FRA9A is evident when compared to the non-fragile Chr9 from the same metaphase spread (Figure 4A, control Chr9 in lower left is from the same metaphase as the left-most stretched FRA9A). These cytogenetic observations reveal a fragile site, FRA9A, at 9p21.

We next quantified fragility. Established FXS/FRAXA diagnostic guidelines (93,94) dictate that fragile site frequencies of 3% or 5% within 100 metaphases yields confidence levels of 95% or 99%. Typically, FXS individuals show fragility at 3–15% but never >50% of CGG expanded ChrXs (94,95). We observed 9p21 fragility at 7–14% across *C9orf72*Exp cell lines (Figure 4E). Fragility was evident in *C9orf72*Exp cells of presymptomatic and ALS/FTD-affected individuals. Chromosomal assignment and band location of fragility was confirmed by Giemsa-banding, trypsinization and karyotyping (Supplementary Figure S3). Fragility at 9p21 was observed on only one of the Chr9 homologs in a given metaphase of any one *C9orf72*Exp cell line, consistent with each being heterozygously expanded. Fragility at 9p21 was only detected with FUDR treatment. Similar levels of fragility arose using folate-free media (M199) as for FUDR, revealing induction by different methods of folate stress (Supplementary Figure S3A). Fragility could not be induced without *C9orf72* expansions in two control cell lines (100 metaphases each). Thus, fragility depends on folate perturbation and the presence of the expanded repeat. As few as 300 repeats (P3, 9%) could express FRA9A at similar levels as 4400 repeats (P4, 8%). The localized fragility, limited to one Chr9, in *C9orf72*Exp cells is consistent with previous FS mapping to autosomes that concluded fragility arises on the expanded allele (96,97). We validated that the *C9orf72* repeat expansion is the molecular cause of FRA9A fragility through gene-transfer experiments (below).

We further mapped fragility using seven FISH probes spanning the outer edges of 9p21, in eight *C9orf72*Exp cell lines, >100 metaphases each, with probe signals being telomeric, spanning or centromeric to the break (Figure 4B, D and F). Breaks were detected across 9p21.1–9p21.3 chromosomal bands, ~8.2 Mb, with ≥83% of breaks at a ~1 Mb stretch of 9p21.2 encompassing *C9orf72* (Figure 4D). Splitting of the FISH signal to both sides of the break was evident for the GGGGCC-containing probe 4, supporting that the expanded repeat causes fragility (Figure 4C). Probes telomeric to *C9orf72* preferentially fluoresced telomeric of the break, with the same trend for centromeric probes (Figure 4F). The

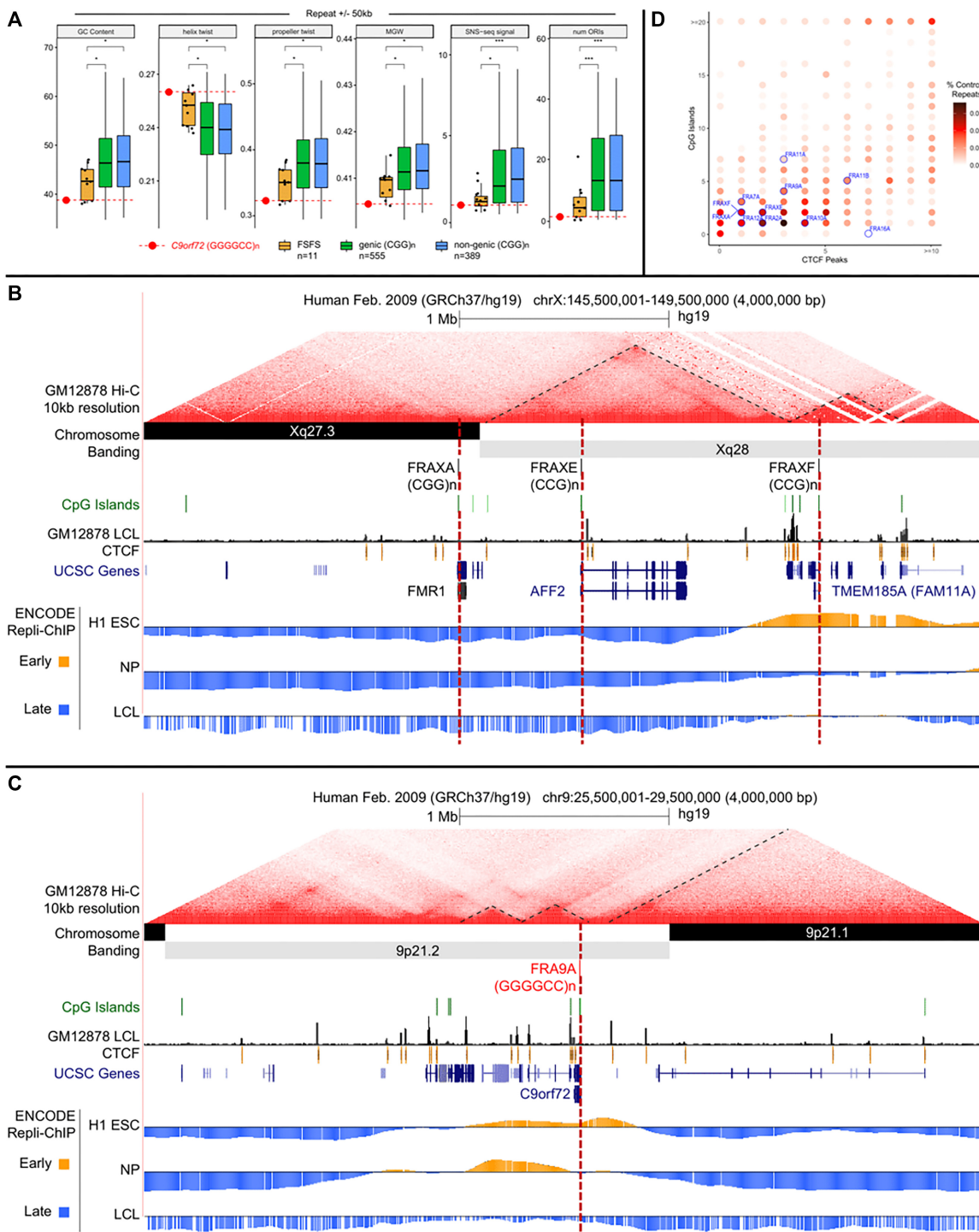


Figure 2. DNA sequence, structure, topological-associated domain (TAD), CpG island and Repli-Chip analysis for all 10 CGG-FSFS. **(A)** Boxplots comparing average %GC, helix twist, propeller twist, major groove width (MGW), SNS-seq (short nascent strand sequencing) signal and number of origins of replication initiation (ORIs) at CGG/CCG-mapped FSFS and *C9orf72* versus 944 control genome-wide CGG/GGC repeats, calculated for windows ± 50 kb and ± 500 kb from the repeat center. Control repeat regions were further separated as genic or non-genic based on overlap with an annotated transcript. Median repeat length for FSFS is 8.7; all FSFS have GC content of 100% (AT = 0 except FRAXF, GC = 0.826). Repeat length req of >4.5 for 944 CGG/CCG control regions yielded a median length of 8.7, same as mapped FSFS. Asterisk denotes significance based on a two-sided Wilcoxon test (* $P < 0.05$; ** $P < 0.01$). Each individual FSFS is represented as a black dot. The *C9orf72* (GGGGCC) $_n$ is represented by a red dot. **(B** and **C)** Topological domain, DNA replication timing tracks, CpG islands and CTCF sites for the contiguous FRAXA, FRAXE and FRAXF compared to the same for *C9orf72*. Shown are the contour density plots depicting the number of CTCF sites and CpG-islands in 100 kb windows centered on the repeat, representing boundaries with normal-length, matched repeats. Repli-seq data were obtained in bigwig format (GSE61972). H1 ESC = H1 Embryonic Stem Cells; accession:ENCF000KUF; NP = Neuronal progenitor cells (BG01 Fibroblast-derived); accession:ENCF907YXU; LCL = GM06990 lymphoblastoid cells; accession:ENCF000KUA. Early (positive) and late (negative) replication was determined by subtracting the genome-wide median score from all values. To conserve space, only the FSFS gene is indicated, while other UCSC genes are condensed into one line. **(D)** Summary of enrichment of each fragile site (indicated in blue fonts) for CpG islands and CTCF sites. Points are colored according to density. For analyses of FRA2A, FRA7A, FRA10A, FRA11A, FRA11B, FRA12A and FRA16A, see [Supplementary Figure S1](#).

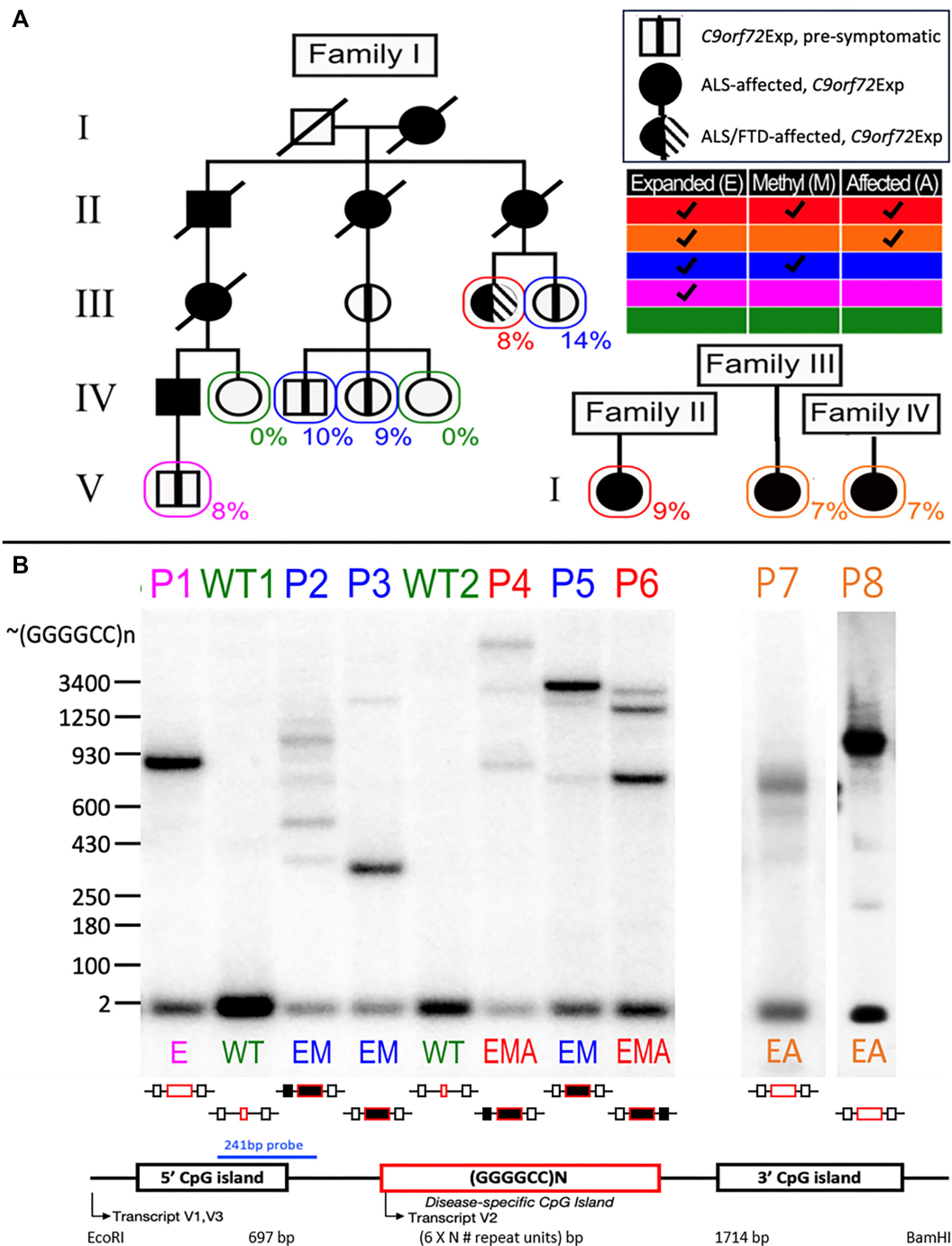


Figure 3. *C9orf72*Exp cells, repeat lengths, CpG-methylation and disease state. **(A)** ALS/FTD families with Southern blot vertically aligned for each individual. Females are represented by circles, males by squares, and disease state is as per the insert legend. Colors of text and boxes around symbols indicate the expansion, methylation and affected status for each sample. Percentages of cells showing FRA9A expression are indicated for each individual in the pedigree. 'P#' refers to patient number, 'E', 'M' and 'A' refer to Expanded, Methylated and Affected, is summarized at right, and this coding system is used throughout the text. Southern blot of *C9orf72* (GGGGCC)_n repeat expansion ('Materials and methods' section) used EcoRI/BamHI to release the repeat-containing fragment leaving 697 and 1714 bp upstream and downstream of the (GGGGCC)_n/N repeat. **(B)** Schematic of Southern blot probe location, CpG-methylation status at the GGGGCC repeat and CpG-islands (filled boxes denote methylation). For raw CpG methylation data, see [Supplementary Figure S2](#).

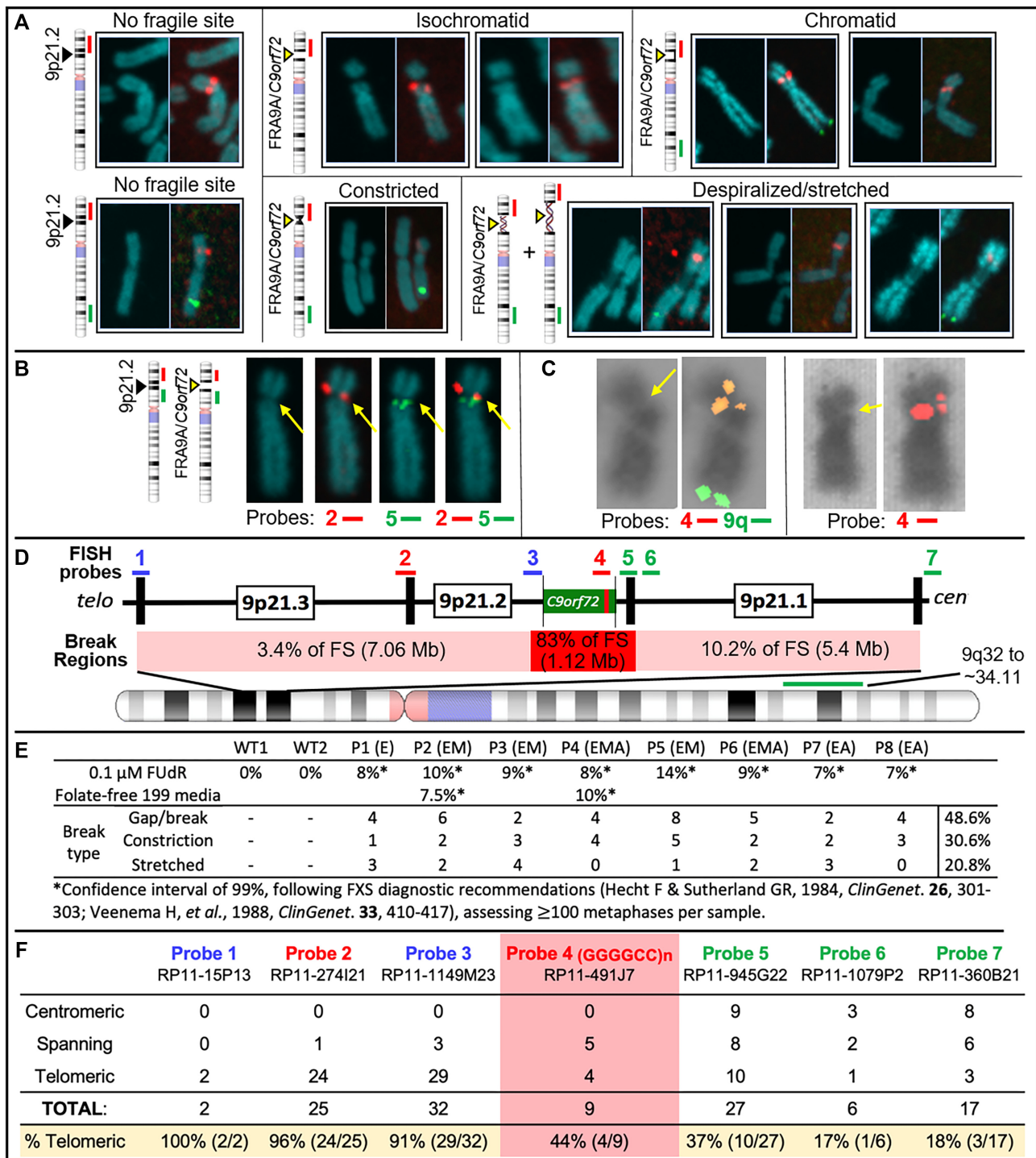




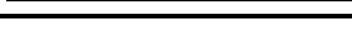






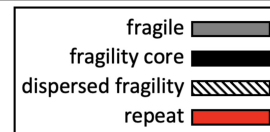
Figure 4. *C9orf72*Exp causes FRA9A folate-sensitive fragile site that maps across 9p21. (A) Fragile site forms (indicated), with examples of non-fragile chromosomes from the same metaphase spreads. Showing DAPI-stained and paired FISH-probed chromosomes from FUDr-treated cells. 9q-arm FISH probe (9q32~34.11; RP11-696J10) in green. FISH probe #2 at *C9orf72* (panel D-F) in red. Magnification is the same for all chromosome images within each panel, facilitating comparison within the panel. Control Chr9 in upper left of panel (A) is from the same metaphase as the leftmost isochromatid Chr9. Full metaphase spreads can be provided upon request. Notably, the control 'No fragile site' Chr9 in lower left of panel A is from the same metaphase as the leftmost 'Despiralized/stretched' Chr9, revealing the lengthening of the same chromosome (same magnification) with or without indicated FISH probes. (B) Representative example of the same chromosome (same magnification) with or without indicated FISH probes. (C) Two representative examples (same magnification) of isochromatids with FISH signal of *C9orf72*-containing probe 4 split over the fragile site. (D) 9p21 location of FISH probes with regional summary of fragile site location. (E) Quantification of fragility for ≥100 metaphases under two folate-stressed conditions. (D) Cells were described in Figure 3. (F) Fragile site breakage regions calculated from number of breaks relative to FISH signal found centromeric, telomeric or spanning across probes used. Percentage of telomerically located FISH signal relative to the break is on the bottom row. Frequencies of probes found spanning or on each side of the break were used to calculate the percent breakage within each region in panel (D).

Table 1. Large fragile sites with variably located fragility cores (increased breakage) and gene numbers

Fragile site	location	fragility size	fragility core size	core location	# genes*	TEL	schematic; — = 1 Mb	CEN	citation
FRA1H	1q41-42.1	10 Mb	4 Mb	asymmetric	49			75	
FRA3B	3p14.1-14.2	4 Mb	500 kb	asymmetric	24			77	
FRA4F	4q22	7 Mb	4 Mb	broad	12			76	
FRA7B	7p21.3-22.3	12.2 Mb	5 Mb	asymmetric	79			73	
FRA9E	9q32-33	9.8 Mb	5 Mb	broad	63			74	
FRA9A	9p21	8.2 Mb + repeats**	500 kb + repeats**	asymmetric	46			this study	
FRA11G	11q23.3	4.5 Mb	2.32, 1.37 Mb	broad	38			78	
FRAXA	Xq27.3	20-600 kb + repeats**	20 kb + repeats**	centric	10			79, 80	
FRAXF	Xq27-q28	1-2.5 Mb + repeats**	1 Mb + repeats**	asymmetric	110			81, 82	

*The number of genes in the fragile region was determined for protein-coding genes as of 01-2024 as per FISH probes used.

**Schematic of FRA9A, FRAXA, and FRAXF is shown with (GGGGCC)4000, (CGG)900, and (CCG)600 repeats, respectively (red bars).



telomeric boundary could be considered at probe 2, which straddles 9p21.2–9p21.3, with fluorescence both telomeric and spanning fragility. A centromeric boundary could not be defined, as probe 7 was detected telomeric, spanning and centromeric to breaks, suggesting fragility extended centromeric of probe 7. Additional centromeric probes, being pericentromeric, hampered break detection. Thus, within the limits of FISH resolution, FRA9A maps most intensely to *C9orf72*, but has a wide zone of breakage (summarized in Figure 4D). FRA9A's fragility core of enriched breakage includes *C9orf72* covering ~500 kb (plus the repeat), spanning the *C9orf72Exp* risk haplotype, where breaks can extend ~2 Mb and ~6.2 Mb telomerically and centromerically (Table 1). This makes FRA9A one of the largest fragile sites, spanning ~8.2 Mb over 9p21.1–21.3, encompassing 46 genes (Table 1), similar in size to FRA1H, FRA3B, FRA4F, FRA7B, FRA9E, FRA11G and FRAXF, spanning up to 12.2 Mb over multiple chromosome bands, encompassing 10–110 genes (Table 1) (98–107). Moreover, CpG-methylation of *C9orf72Exp* was not required, as fragility was observed in cells \pm methylation (Figure 4E). Thus, neither symptomatic state of blood donors nor CpG-methylation were required for FRA9A expression. That we detected FRA9A fragility at 9p21 in *C9orf72Exp*, lymphoblastoid cells, confirms previous observations that FRAXA expression was similarly detected lymphoblastoid cells as in freshly-collected peripheral blood lymphocyte cultures (108). Thus, FRA9A and FRAXA are distinct from the fragility at 11q23, which depends upon the EBV encoded protein EBNA1 (109–112).

C9orf72Exp allele assumes a compact chromatin conformation, which is enhanced by expansion size and CpG-methylation

Since constricted fragile sites on metaphase chromosomes may be the result of localized unusual chromatin condensa-

tion, we next determined whether the mutant *C9orf72Exp* locus assumes an unusual chromatinized state relative to the non-mutant allele using micrococcal nuclease (MNase) accessibility, which is widely used as an indication of regional chromatin compaction. We were able to electrophoretically resolve MNase accessibility on the mutant from the non-mutant alleles by Southern blotting. MNase can directly reveal both inaccessible and accessible regions for each allele, while sequencing-based methods of chromatin accessibility, like ATAC-seq, must impute inaccessibility and cannot resolve alleles. Permeabilized cells were exposed to MNase, which preferentially cuts DNA between nucleosomes; DNA was de-proteinized, isolated, restriction digested releasing the repeat-containing fragment, electrophoretically resolved and detected by the Southern blotting (Figure 5A and B, blue probe). Over-digestion by MNase to mono-, di- and trinucleosome sized DNA fragments was evident by ethidium staining (Figure 5C, left panel). A striking resistance to MNase accessibility is seen exclusively for the *C9orf72Exp* allele, contrasting the non-expanded allele, which serves as an internal equimolar control, completely degraded at low MNase concentrations (Figure 5C, compare lanes 4 and 5). The expanded allele resisted digestion at much higher MNase concentrations (Figure 5, compare lanes 5–10). MNase resistance extended beyond the expansion into the flanking regions of the mutant allele. Increasing concentrations of MNase (>50 Units) led to partial and progressive degradation of the expanded allele to a distinct shorter size, losing ~1 kb of flanks from the full-length EcoRI-BamHI restriction fragment, which subsequently digested the probed region (Figure 5C, schematic). Conversely, on the non-mutant allele, the same flanking regions and non-expanded repeat were completely digested at low MNase concentrations, along with the rest of the genome (<10 Units, Figure 5C, lanes 5–10). The poor digestion of the *C9orf72Exp* mutant allele relative to the internal sequence control of the equimolar non-mutant allele

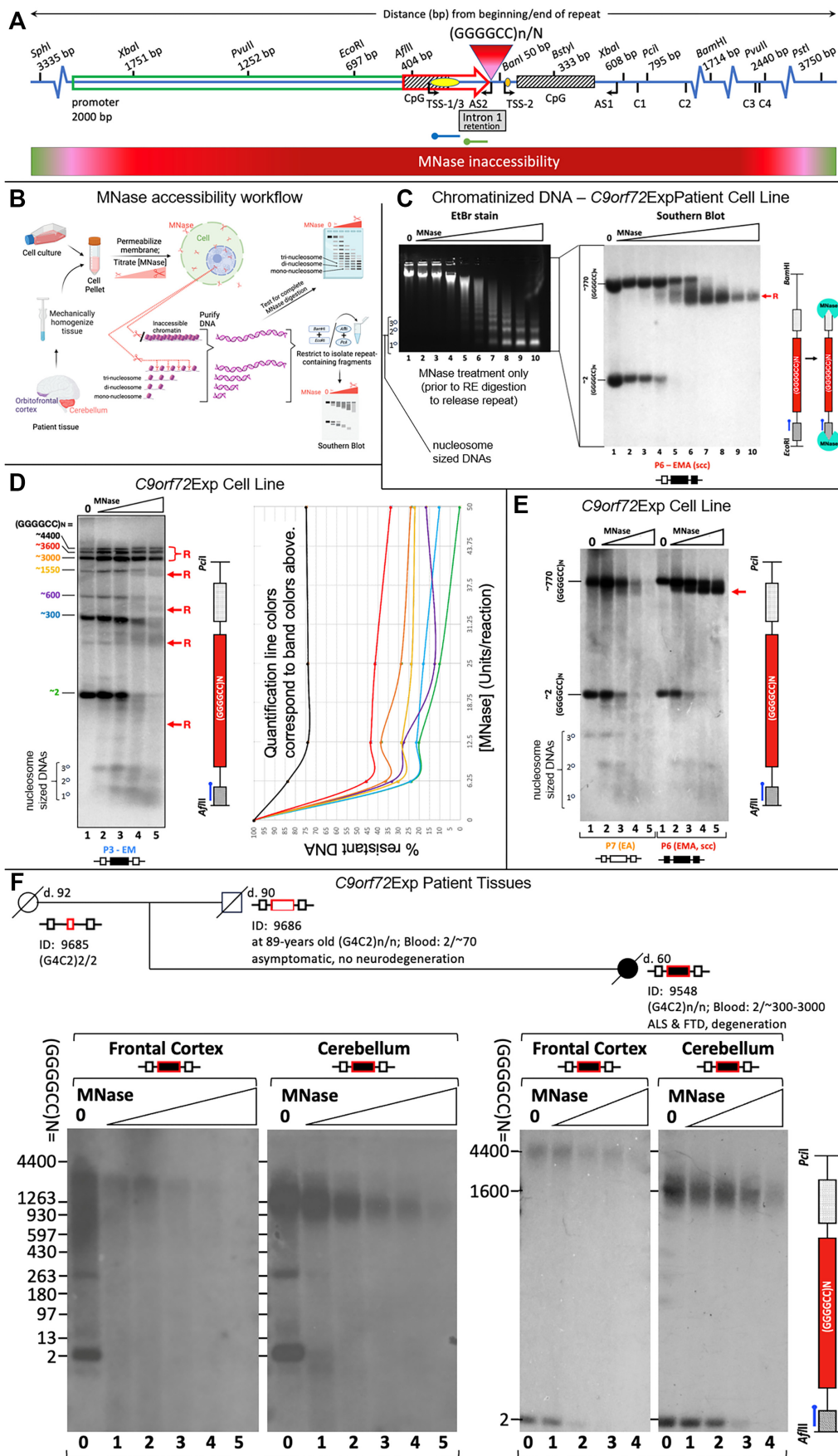


Figure 5. *C9orf72*Exp locus is MNase-inaccessible. (A) Schematic of the region of unusual chromatin organized as determined by MNase accessibility analysis in *C9orf72*-ALS patient cells and brain regions. *C9orf72* (GGGGCC)n-N repeat, CpG-islands (hatched boxes), long-2 kb and intermediate 435 bp

strongly suggests the formation of an unusual chromatinized state of the mutant *C9orf72* allele. Control experiments confirmed that the inaccessibility of MNase to the *C9orf72*Exp allele was due to its chromatinized state, and not due to an inherent inability of MNase to cleave the expanded non-chromatinized (GGGGCC)_n sequence (Supplementary Figure S4A and B, ‘Materials and methods’ section). Six cell lines showed MNase resistance of the *C9orf72*Exp allele, regardless of presymptomatic or symptomatic state of the blood donors (Figure 5C–E).

Mapping the boundaries of MNase-resistance using multi-probe and multi-restriction digests revealed the extent and distribution of MNase inaccessibility over the *C9orf72*Exp allele. Maximal MNase resistance spanned a total of >33 kb for an allele with 4400 repeats (P4), with MNase inaccessibility extending ~3300 bp upstream and ~3700 bp downstream of the repeat (summarized in Figure 5A to scale, Supplementary Figure S4C, see ‘Materials and methods’ section). Mapping in six *C9orf72*Exp cell lines showed little variation of the absolute boundaries of MNase inaccessibility with expansion size or presence of disease. Together, these data confirm that the *C9orf72*Exp allele assumes a large region of compact chromatin. Maximal MNase inaccessibility covers the upstream CpG-island, the *C9orf72* promoter, transcription start sites (sense and anti-sense), the expanded repeat, cryptic splice sites C1–4, the downstream CpG-island, beyond exon 2, and falls within FRA9A’s fragility core.

Repeat length and CpG-methylation enhanced MNase-resistance. Analysis of a cell line that harbored a mosaic heterogeneous mixture of expansion sizes ranging between ~300 and 4400 repeat units demonstrated that repeat expansion size directly correlates with MNase resistance (Figure 5D, P4). Longer expansions were more resistant to MNase than shorter expansions, which were more resistant than the non-expanded alleles (Figure 5D, lanes 3 and 4, quantified in Figure 5D). CpG-methylation exacerbated inaccessibility. Two cell lines with similar expansion sizes (~770 repeats) with or without aberrant methylation at the mutant *C9orf72* (P6 [isolated single cell clone] and P7, respectively) showed that methylation further enhanced MNase resistance of the expanded allele (Figure 5E and Supplementary Figure S4A, iii). Larger expansions and methylation enhance chromatin compaction of the *C9orf72* locus.

We assessed chromatin compaction of post-mortem brains of two *C9orf72*Exp individuals, previously deep-phenotyped for lifestyle choices, clinical, neuropathological, molecular and genetic biomarkers (29,70). One was a 90-year old male asymptomatic for ALS or FTD, with a distinct ~70 repeats in blood, no signs of neurodegeneration, overexpression of *C9orf72*/*C9ORF72* and devoid of TDP-43 neuropathology (summarized in Supplementary Table S2). The other was his daughter with 300–3000 repeats in blood who had ALS at age 57 and died at 59 and autopsy showing neurodegeneration and TDP-43 inclusions (29) (detailed in Supplementary Table S2). The asymptomatic father had a striking heterogeneous mosaic range of 13–3500 and 13–1500 repeats in the frontal cortex and cerebellum, respectively, with CpG-methylation likely triggered by large (>70 repeats) expansions (Figure 5F, lanes 0). In contrast, the affected daughter showed very large distinct expansions of mostly ~4400 and ~1600 CpG-methylated repeats in the frontal cortex and cerebellum, respectively, where the intensity of the expansions matched that of the non-expanded allele (Figure 5F, lanes 0). Chromatin was MNase inaccessible on only the expanded *C9orf72* alleles in both brain regions of both individuals, while the non-expanded (GGGGCC)₂ allele was rapidly digested by MNase (Figure 5F). MNase inaccessibility for both individuals appeared more severe in the cerebellum relative to the frontal cortex, which contrasts the expectation that the longer expansions in the frontal cortex would make it more MNase resistant, but may reflect the longer expansions and/or the increased levels of deacetylated and trimethylated histone modifications in the frontal cortex over the cerebellum, relative to the acetylated histones on the non-expanded allele of *C9orf72*Exp carriers (113). The shorter expansions in the father’s brain were more MNase sensitive than the larger expansions. Quantifying MNase inaccessibility between asymptomatic and symptomatic brains is hampered by the repeat length variations they presented, which we have shown to affect chromatin accessibility (Figure 5D). Expression of the *C9orf72* transcript in the asymptomatic *C9orf72*Exp father was dramatically increased 2.5- to 7-fold in the frontal cortex, cerebellum, spinal cord, blood and four other tissues compared to the affected daughter’s tissues, whose *C9orf72* levels were twice less than an individual devoid of expansions (29,70). We suggest that the increased transcription in the father’s brain arose from the shorter range of expansion sizes

promoters (green and red arrows, respectively), exons 1a (yellow dot) and 1b (orange dot), sense and antisense transcription start sites, restriction sites with distances from the beginning and end of the (GGGGCC)_N tract, and probes for upstream (green) and downstream (blue) mapping of MNase accessibility. Cryptic splice site transcripts C1–C4 derived from the *C9orf72*Exp allele are indicated with their distance from the end of the repeat tract (42,45). (B) Workflow for MNase assay. (C) MNase treatment of chromatinized DNA from a cell line (P6) with a large methylated *C9orf72*Exp that had undergone single-cell cloning (scc) to isolate a single expanded allele, ensuring a single expansion size and facilitating clarity. EtBr staining of the MNase-treated DNA reveals over-digestion of the DNA to mono-, di- and tri-nucleosomal, sized fragments. The same DNA was digested with EcoRI/BamHI, to release the repeat fragment having 697 bp upstream and 1714 bp downstream of the repeat, then assessed by Southern blotting using the blue probe. Resistance of only the expanded allele occurs, even at high concentration of MNase (200U). Red ‘R’ indicates the region with reduced MNase accessibility that is about to lose the probed region indicated in the schematic at right. (D) Sample P3 with a mixture of heterogeneous repeat allele lengths shows that with increasing repeat size, MNase accessibility is decreased, as quantified by densitometric analysis for each allele size (colours coordinate between graph and Southern blot). In panels D–F the repeat was released with AfIII/PciI, leaving 404 bp upstream and 689 bp downstream allowing increased resolution. NB, van Blitterswijk uses XbaI/XbaI to release the repeat, leaving 1751 bp upstream and 608 bp downstream of the repeat, the greater amount of flanking sequence reduces electrophoretic resolution. (E) Methylation is associated with increased MNase inaccessibility as assessed in cell lines (P6 [sssc] and P7) containing similar sized repeats but differing methylation status. The non-expanded allele is digested at the same rate in both lines. (F) MNase treatment of post-mortem (orbito)frontal cortex and cerebellum from an asymptomatic 90-year-old father and his ALS-FTD-affected daughter, previously deep-phenotyped for lifestyle choices, clinical, neuropathological and molecular biomarkers (29,70) (summarized in Supplementary Table S2). MNase concentrations are doubled between each lane (2.5U in lane 2 up to 40U). Expanded allele in both tissues is MNase resistant relative to the equimolar non-expanded allele, which serves as an internal control. See Supplementary Figure S4 for MNase controls and mapping experiments.

(13–1200 repeats) which were less MNase resistant than the longer expansions, which is consistent with both the over expression in the father's blood, which contained predominantly 70 repeats, and with the low transcription in the daughter's brain that contained only very large expansions. This interpretation is consistent with the 2.5- to 5-fold increased expression of intermediate *C9orf72* repeats in human brains, blood and knockin induced pluripotent stem cell- (iPSC-) derived neural progenitor cells (91,114). This parallels the 5- to 10-fold increased expression from the premutation CGG expansions at the *FMR1* repeat in hemizygous males, which also show compact chromatin (115,116). We conclude that *C9orf72* expansions and flanks assume a highly compact chromatin in cells and brain regions of *C9orf72*Exp carriers. MNase resistance is evident on all *C9orf72*Exp alleles in a given sample, which differs from the 7–14% of *C9orf72*Exp cells cytogenetically showing FRA9A-Chr9s, like FXS, only a portion of the CGG-expanded Chr9s show FRAXA (94,95). In this manner, MNase resistance might be considered a proxy for fragility. Towards assessing whether MNase resistance was linked to the unusual chromatin compaction of cytogenetic fragility or merely linked to expanded repeats, we assessed the MNase accessibility of the *HTT* locus in Huntington's disease patient cells with (CAG)21/180, which is known to not be a cytogenetically detectable fragile site (117). MNase treatment and Southern blotting resolved the mutant and non-mutant *HTT* alleles and both showed the same MNase accessibility when most of the genome was sensitive (Supplementary Figure S5, lanes 3–5), suggesting that MNase inaccessibility does not extend to this non-fragile mutant locus. As part of another study, we extended the MNase inaccessibility to the CGG-expanded *FMR1* gene the molecular cause for the fragile site FRAXA. We find MNase resistance of only the CGG expanded allele (in cells from male and female carriers of the CGG expansion) (not shown). That the CGG expanded *FMR1*, which forms FRAXA, but not the non-fragile CAG expanded *HTT*, forms an MNase resistant region supports our suggestion that MNase inaccessibility of the *C9orf72*Exp can be considered a proxy for chromosomal fragility. We suggest that the MNase resistance of the *C9orf72*Exp locus in human brains is a reflection of chromosomal fragility (Figure 5F).

Increased Chr9-containing micronuclei in *C9orf72*Exp cells

MN are indicators of chromosomal double-strand breaks (DSBs) including fragile sites (118,65–66,68), where MN often harbor broken chromosomes to be eliminated or reintegrated. NBuds are chromatin-containing protrusions linked to the nucleus by a nucleoplasmic stalk (65,66). Both MN and NBuds can arise from chromosome breaks. NBuds can become MN (65). These subnuclear structures can be enriched with tandem gene amplifications and satellite repeats (92,119–120). Cytoplasmic release of MN DNA triggers an immune response via DNA sensing by cGAS-STING that activates *IFN* expression (118), a pathway hyperactivated in vulnerable neurons of *C9orf72*Exp carriers (4,12–14). Given these connections, we assessed MN and NBuds and whether they contained Chr9 in *C9orf72*Exp cells. *C9orf72*Exp cells showed elevated MN/NBud levels compared to control cells, which were further increased with folate stress (Figure 6A). More NBuds over MNs contained Chr9 in *C9orf72*Exp cells compared to control cells. The modest increase in MN with

Chr9 could be due to loss of fragile chromosome-containing MN during folate-perturbation, as suggested for FRAXA cells (Figure 6B) (121,122). Depending upon whether the breakpoint is centromeric or telomeric of *C9orf72*, the presence of the *C9orf72*-containing FISH signal alone or the 9q-arm FISH signal alone, supports subnuclear inclusion of an acentric or truncated Chr9, respectively, while the presence of both *C9orf72*- and q-arm signals supports the inclusion of truncated Chr9 or the full-Chr9 (Figure 6B). An absence of either FISH signal could reflect an absence of any Chr9, or an acentric Chr9 broken telomeric of *C9orf72*. When Chr9 signals were present in MN/NBuds, the proportion of the *C9orf72* signal alone, 9q-arm alone, or the two together occurred at 1:1:5, respectively. Increased Chr9-containing MN/NBuds were evident in *C9orf72*Exp cells of presymptomatic and symptomatic individuals. Cumulatively, these data support increased chromosomal damage in *C9orf72*Exp cells.

We also observed increased nuclear blebs (NBlebs) in *C9orf72*Exp compared to control cells (Figure 6A). NBlebs are chromatin-containing nuclear herniations (65–66,123–124), without an obvious constriction between the nucleus and the protruding nuclear material. NBlebs may in some instances lead to NBuds, which may lead to MN (65). NBlebs are hallmarks of the DNA damage accumulating progeroid syndromes and can be enriched with genomic regions with perturbed chromatin and DNA damage (γ H2AX) (123–127). In *C9orf72*Exp cells, NBlebs contained Chr9 at higher levels than in cells without expansions (Supplementary Figure S6A), which is consistent with reports of NBlebs being enriched with regions having altered chromatin compaction and damaged DNA (123–125).

*C9orf72*Exp and double-strand breakage

Direct support that fragile sites are prone to DNA breakage is the cytogenetic manifestation of a truncated chromosome or acentric chromosome fragment broken at the fragile site (128,129). We observed truncated Chr9s broken at 9p21, where the truncated p21→pter acentric arm, containing the *C9orf72*-FISH signal, remained within the same metaphase spread (Figure 6B). We observed numerous instances of truncated Chr9s with the *C9orf72* signal at the broken end, in the absence of their acentric p21→pter acentric arms, which had likely been lost. 9p21-truncated Chr9s without *C9orf72*-signal were also observed, consistent with FRA9A's broad ~8.2 Mb breakage zone (Figure 6B, see truncated Chr9 broken centromeric and telomeric of the *C9orf72*-FISH signal). Our cytogenetic findings, coupled with the increased Chr9-containing MN/NBuds, is convincing evidence that double-strand DNA breaks occur at FRA9A, consistent with the γ -H2AX foci in cells, spinal cord and brains of *C9orf72*Exp carriers (23,24).

We further explored the susceptibility of GGGGCC repeats to double-strand DNA breaks using a yeast system that quantifies rates of chromosome end-loss (69). A (GGGGCC)60 inserted into a yeast chromosome was extremely unstable, yielding mixed populations with 15–60 repeat units (Supplementary Figure S7A–F). Rates of breakage showed a significant length-dependent increase: Tracts of 35–60 repeats broke 6–16-fold more frequently compared to (GGGGCC)15, which incurred breaks at 10-fold higher rates than a (CAG)85 tract analyzed in the same assay (Supplementary Figure S7B and C). Thus, even short GGGGCC repeats can be highly

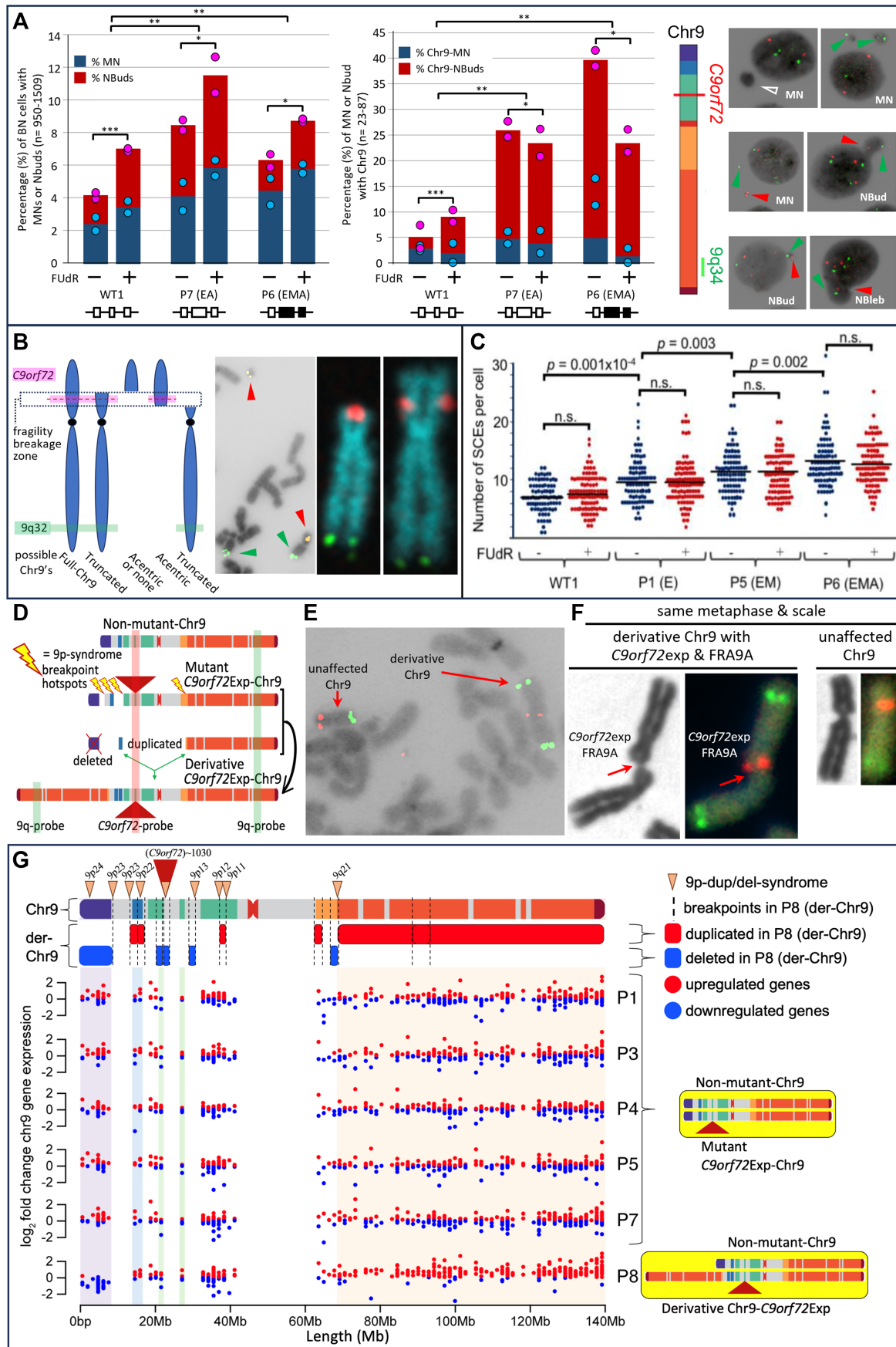


Figure 6. *C9orf72*Exp cells display chromosomal instability. (A) Quantification of MN and NBuds in binucleated cells without FISH, left, and with *C9orf72* and 9q-FISH probes, middle, in WT and *C9orf72*Exp cells (P6 (ssc) and P7) containing similar sized repeats (~770) but differing methylation status. Data

prone to DNA breakage. Instability of a (GGGGCC)₇₀ tract in humans was reported (29).

Sister-chromatid exchange and recombinant events in *C9orf72* expansion cells

An increased incidence of SCEs occurs at rare and common fragile sites (130). We analyzed SCE formation in *C9orf72*Exp. Unexpectedly, *C9orf72*Exp cells exhibit an increase, up to 2-fold, in spontaneous genome-wide SCEs/cell (~7 up to 10–15/metaphase), compared to control cells without expansions (Figure 6C). Increased SCEs were evident in *C9orf72*Exp cells from presymptomatic and symptomatic individuals (Figure 6C, compare P1, P5 with P6, all greater than WT). The increased SCEs did not require FUDR. This increase is significant, yet modest relative to 10-fold increased SCE/metaphase in individuals with the chromosome instability Bloom syndrome. Bloom individuals present high SCEs (131–134), increased MN (132,135), a self-DNA cGAS-STING-mediated *IFN* over-expression (135), and often succumb to cancer before age 30 due to a coincident 10-fold increased mutation rate (134,136,137). Chemical and genetic factors can drive SCEs (134,138,139). In all instances, SCEs predominantly occur at common (140–142) and rare fragile sites (130,143–146), regardless of whether the fragile site is being induced or not (142,147). Consistent with this, the SCEs levels in *C9orf72*Exp cells were mildly but not significantly increased by FUDR (Figure 6C). Through FISH mapping SCEs were significantly enriched on Chr9p, where *C9orf72* resides (Supplementary Figure S6B–D). Thus, the GGGGCC-expanded FRA9A, like the CGG-expanded FRAXA, the AT-repeat-expanded FRA16B, and the EBNA1-motif repeat 11q23 fragile site, incurs increased SCEs (110,112,130,146,148). These findings extend the forms of genetic instability and the sources of DNA damage in *C9orf72*Exp cells to include global and focal SCEs.

Unexpectedly, one of the *C9orf72*Exp cell lines (P8) showed complex rearrangements restricted to one Chr9, clearly evident in every metaphase (100/100 observed) (Figure 6D–F). Specifically, one Chr9 showed a duplication of nearly the entire 9q-arm (9qter-q21.11 fused to 9p23, Figure 6C), a terminal deletion of 9pter-p23, and duplications of 9p23, 9p12, 9p11.2, 9q13, 9q21.11, and deletions in 9q13, making a derivative-Chr9 (see CNV and whole-genome sequencing analysis, Figure 6D–E; Supplementary Figure S8A and Supplementary Table S3). Breakpoint pattern was reminiscent to 9p deletion/duplication syndrome (Figure 6G, top

(55,149). Importantly, only the derivative-Chr9 expressed FRA9A with FUDR in 7% (7/100) metaphases (Figure 6F), indicating it arose from the *C9orf72*Exp Chr9. Strikingly every metaphase showed the same rearrangements, which were evident prior to FUDR treatment. In our previous examinations of thousands of metaphases from control cells, we have not observed such homogeneity of rearrangements, making it highly unlikely that this derivative-Chr9 arose by cell line establishment or culturing. It is also highly unlikely that this individual, who was neurotypical until presenting with bulbar onset ALS at age 56, had inherited this complex set of rearrangements constitutionally in all tissues, as congenitally such rearrangements would be incompatible with neurotypical life (55,149). Rather than inherited, it is likely the rearrangements arose somatically in the blood of the *C9orf72*Exp individual, which is supported by our observation of similar rearrangements of the *C9orf72* transgene-containing Chr6 in mouse tissues (below). Whole genome sequencing revealed the derivative-*C9orf72*Exp-Chr9 presented a unique state with ≥ 13 breakpoints clustered on 9p, with direct and inverted junctions, confined to a single chromosome, as such, fulfilling the criteria of chromothripsis (150–152). It is possible the FRA9A-expressing *C9orf72*Exp-Chr9 isolated in a micronucleus, was shattered and reassembled as the derivative-Chr9 (153). A single experimentally targeted DSB can induce chromothripsis to the targeted chromosome (154,155). The derivative-Chr9 may have arisen by stepwise alterations. The origin of the derivative-*C9orf72*Exp-Chr9 could not be discerned as the patient was deceased. The complex chromosomal rearrangements of the mutant *C9orf72*Exp FRA9A-expressing Chr9 could have downstream impact.

While we cannot exclude the possibility that the highly rearranged derivative-Chr9 in the *C9orf72*Exp cell line (P8) arose during cell line establishment or passage, it is difficult to argue away the coincidences that the rearrangements we observe were limited to only one Chr9—the Chr9 with the *C9orf72*Exp expressing FRA9A (Figure 6D–F), and that the breakpoints were non-random but aligned with the breakpoints of 9p-duplication/deletion syndrome (Figure 6G) (55). We also observed numerous forms of chromosome rearrangements of murine chromosomes harboring the human *C9orf72* expansion, including one reminiscent of the der-Chr9 we observed in the human cell (see murine cytogenetics described below). Moreover, the cytogenetic observation of thousands of human EBV-transformed cells have not presented such chromosomal instability (59), besides from the EBV-induced

are means of two independent experiments. Dots show data of each experiment. Statistical analyses using Fisher's exact test (* $P < 0.05$, ** $P < 0.01$, *** $P < 0.001$). Representative images of MN and NBuds in cytokinesis-blocked cells treated with FUDR for 24 h that contain no FISH signal (hollow arrows), a *C9orf72*-signal (red arrows) or 9q-signal (green arrows). (B) Depending upon site of breakage, *C9orf72*-FISH probes can have varying interpretations, left. Example of *bona fide* chromosome breaks in *C9orf72*Exp line P4 with acentric terminal *C9orf72*-containing fragment in same metaphase spread as a truncated-Chr9 that is free of *C9orf72*-signal, middle. Example of truncated-Chr9 with *C9orf72*-signal, and control Chr9 from same spread, right. (C) Levels of global SCEs in WT and *C9orf72*Exp cells \pm FUDR. Methylation/clinical status is as per Figure 3. Each datapoint represents a single metaphase. At least 100 mitotic cells were analyzed per condition in each experiment. Statistical analyses were performed by Student's t-test ($P < 0.01$). NS: not significant. See also Supplementary Figure S6B and D. (D) *C9orf72*Exp line P8 with complex highly rearranged derivative-Chr9, schematic, see text and Supplementary Figure S7A. (E) Example of FRA9A-expressing derivative-Chr9 and control Chr9 in same spread with *C9orf72*- (red) and 9q-FISH probes (green) (100% = 100/100 metaphases). (F) Only the derivative-Chr9 expresses FRA9A coincident with the *C9orf72*-FISH signal, revealing derivative-Chr9 to be the *C9orf72*Exp-Chr9, (+FUDR, 7% = 7/100, 99% confidence). (G) Breakpoint analysis (top) and gene expression (binned/gene) along Chr9 in each of the *C9orf72* Exp cells with trisomic (red dots) and monosomic (blue dots) in duplicated and deleted regions of the derivative-Chr9 (P8). Breakpoint and copy number change analysis in P8 was by whole genome sequencing, see Supplementary Table S3. An interactive html file detailing mis-expressed genes can be accessed here <https://data.cyverse.org/dav-anon/iplant/home/ljsznajder/FRA9A/Chromosome9.html>, also presented in Supplementary Table S4. See Supplementary Figure S7B–D for statistical significance of differential gene expression.

fragility at 11q23, which depends upon the EBV protein EBNA1 (109–112).

Gene expression across most of the derivative-Chr9 is dysregulated. Expression analysis by RNA-seq comparing P8 to other *C9orf72*Exp cells, revealed trisomic and monosomic expression levels of many genes corresponding to the large duplicated and deleted regions (Figure 6G, see red and blue dots, for significance see [Supplementary Figure S8B–D](#), an interactive html file detailing mis-expressed genes can be accessed here: <https://data.cyverse.org/dav-anon/iplant/home/ljsznajder/FRA9A/Chromosome9.html>), also presented in [Supplementary Table S4](#). Amongst the dysregulated genes along the der-Chr9 in P8, many are also dysregulated in vulnerable neurons of *C9orf72*Exp ALS patients, including ALS- and inflammation-linked genes (<https://www.biorxiv.org/content/10.1101/2023.12.22.573083v1>, [Supplementary Table S4](#)). Breakpoint and copy number changes analyzed in P8 are presented in [Supplementary Table S4](#).

Cell culture in FUDR increases repeat instability

We tested whether repeat length instability could be generated in *C9orf72*Exp patient cells under fragile site inducing conditions. We observed that expansion tracts shifted towards shorter repeat lengths over culture time in FUDR-treated cells ([Supplementary Figure S9](#)). In contrast, under uninduced conditions, the expanded repeat showed a general shift towards longer repeat sizes or the more predominant repeat length ([Supplementary Figure S9](#)). FUDR affected the length of only the mutant *C9orf72*Exp allele. FUDR-induced changes were consistent in three different *C9orf72*Exp cell lines and did not appear to depend upon methylation or clinical status ([Supplementary Figure S9](#)). These results support repeat size variations being generated under folate-perturbing fragile site inducing conditions.

Tissue-specific somatic repeat expansions, chromosomal fragility and chromosomal instability in *C9orf72*Exp mice

Tissue-specific somatic repeat instability, FRA9A chromosome fragility and chromosome instability were recapitulated in *C9orf72*Exp-Transgenic (Tg) mice (*C9orf72*Exp-Tg) harboring a single copy of the human *C9orf72* with a GGGGCC expansion integrated into murine Chr6 (156). Using this mouse as a tool for instability, we isolated cells from various organs of *C9orf72*Exp-Tg and control non-Tg mice, aged 5 months, when cell proliferation in the CNS and peripheral organs had ceased at 2 months of age (77–79) (see ‘Materials and methods’ section). To retain as close a representation of cell types, harvested tissues were cultured for short periods sufficient for chromosome preparation (1–4 weeks, with no storage). Tissues from three mice inheriting ~620–690 repeats (tail at 2 weeks, aged 5 months) showed a heterogenous smear of 586–1488 repeat sizes, with some of the greatest expansions in the CNS (Figure 7A). This supports massive post-natal inter- and intra-tissue repeat expansions in non-proliferating murine tissues, as observed in *C9orf72*Exp humans (26–30). Expansions were evident as early as 2-weeks (Shum *et al.*, in preparation).

Chromosomal fragility of the *C9orf72*Exp transgene occurred in all tissues at frequencies of 5% to > 35% (99% confidence, Figure 7Bi–iii). Fragility presented as despiralized regions, constrictions, chromatid and isochromatid, breaks,

with split transgene-specific *C9orf72* FISH signals, as we observed in human *C9orf72*Exp cells (Figure 5B,i). Only chromosomes from the transgenic mice showed FUDR-induced fragile sites, where fragility localized to the expanded repeat of the integrated transgene, but never to the non-transgenic Chr6 ([Supplementary Figure S10](#)). Thus, FRA9A fragility can be transferred to this Tg-mouse thereby validating the *C9orf72* repeat expansion as the molecular cause of FRA9A.

Chromosomal instability was evident on the *C9orf72*Exp-Tg-containing Chr6, including acentrics, truncations, duplications, translocations, deletions and multi-branched chromosomes (Figure 7C). In one instance the *C9orf72*Exp-Tg translocated itself from murine Chr6 to another chromosome (Figure 7C), and in another the *C9orf72*Exp-Tg was deleted (Figure 7C). We observed a rearranged chromosome with a large duplication (Figure 7C), reminiscent of the derivative-*C9orf72*Exp-Chr9 in ALS patient, P8 (Figure 6D–G). Chromosomal fragility and instability were observed in all tissues of all three *C9orf72*Exp-Tg mice.

While rearranged chromosomes were rare relative to fragility, neither were ever observed in the non-transgenic murine Chr6 at 6qE3, the site of transgene integration, or in any control non-transgenic tissues (three replicate mice). The absence of fragility at 6qE3 in control non-transgenic tissues is consistent with 6qE3 not being an endogenous fragile site in mice (80). Together our data support the ability of the *C9orf72*Exp-Transgene to incur post-natal somatic tissue-specific repeat expansions, display chromosomal fragility and chromosomal instability, as in humans. Our findings provide insight into fragile site expression and rearrangement in the CNS and periphery.

Discussion

Here, we demonstrate that *C9orf72*Exp is the molecular cause of the rare folate-sensitive FRA9A, cytogenetically observed more than four decades ago (58,157). This reveals previously unconsidered avenues to study genotype-phenotype relationships for co-occurring disease states associated with *C9orf72*Exp and attributes linked to the 9p21 region. First, folate-sensitivity suggests a possible gene-environment interaction. Second, FRA9A may serve as a DNA source to activate DDR and *IFN* pathways. Third, FRA9A chromosomal instability and global SCEs may increase somatic mutations at 9p21 and beyond.

Disease penetrance and gene–environment

Gene–environment interactions have long been suspected for ALS, FTD and the incompletely penetrant co-occurring phenotypes of *C9orf72*Exp (158). Folate-sensitive induction of *C9orf72*Exp repeat instability, brain region-specific repeat expansions, FRA9A fragility, chromosomal instability and methylation-sensitive chromatin compaction, which we have shown can arise in cells and tissues of both presymptomatic and symptomatic individuals, may have clinical implications. Lifestyle, including nutritional choices, of *C9orf72*Exp carriers can affect disease onset and progression (40). Proper levels of the linked vitamins B9 (folate) and B12 are protectors from ALS (159). Individuals with folate deficiencies, nutritionally, pharmaceutically or genetically induced, are associated with chromosomal fragility, localized chromosomal rearrangements (160–169), megaloblastic/pernicious

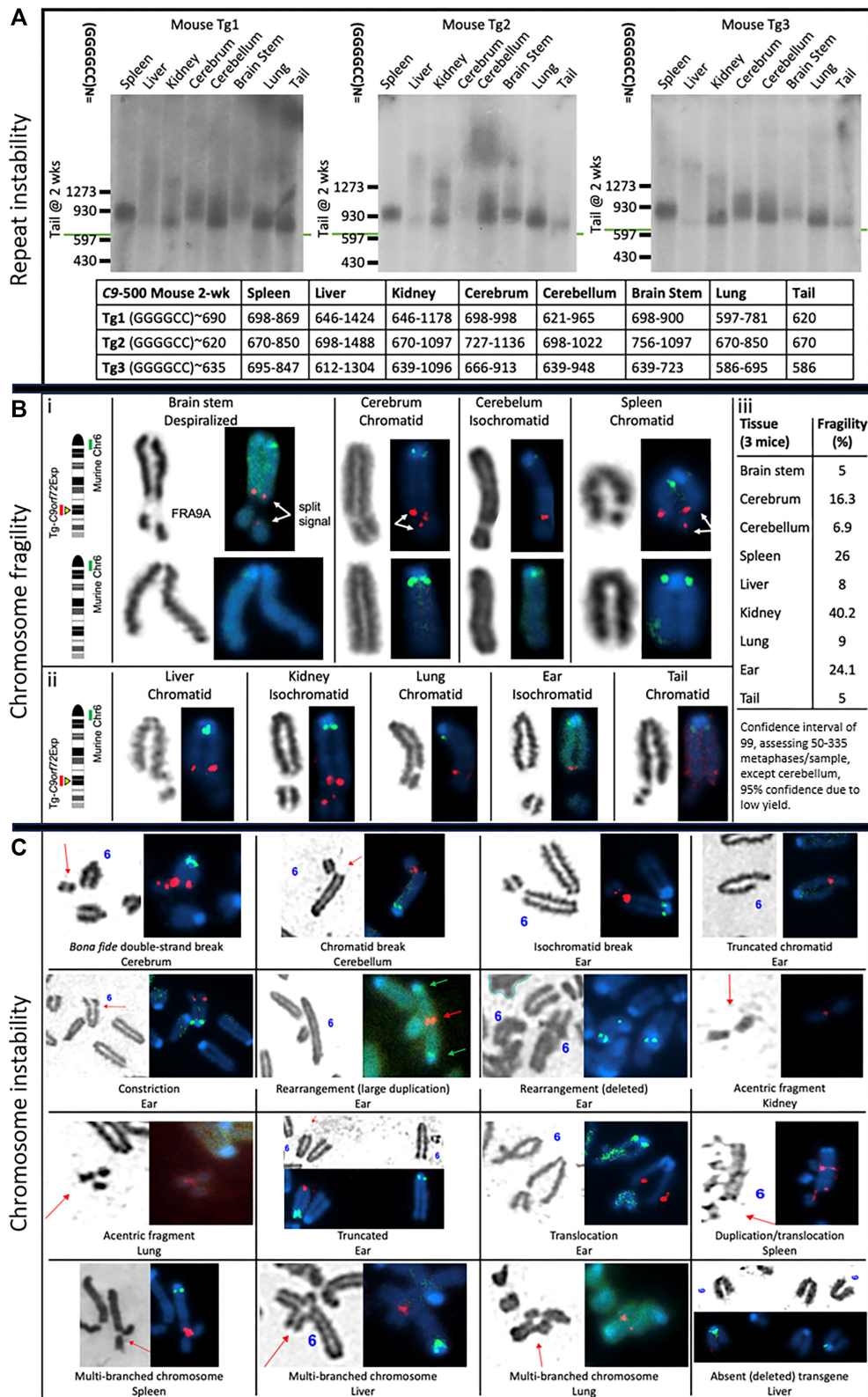


Figure 7. *C9orf72* repeat instability, chromosomal fragility and chromosomal instability in *C9orf72*Exp-Tg-mice. Southern blots for *C9orf72* transgene in C9-500 mouse tissues. C9-500 mouse tissues were sized for repeat size via Southern blot in three *C9orf72*Exp Tg-mice. The tail was the most stable tissue. **(A)** Somatic repeat instability by Southern blots in tissues of three 5-month-old *C9orf72*Exp-Transgenic mice harboring a single copy of the human *C9orf72* gene with a GGGGCC expansion integrated into murine Chr6 (156). **(B)** Cells isolated from tissues of the mice shown in panel (A) were grown for 1–4 weeks sufficient for metaphase spreads for fragility analysis with 1 μ M FUDR with FISH analysis. A murine-specific green probe identified mouse Chr6, and human-specific red probe identified the *C9orf72*Exp transgene. Pictured are FSFS in the CNS (i), the periphery (ii) and quantified in panel (iii). **(C)** Chromosomal instability at the *C9orf72*Exp transgene was assessed in the same tissues used in panel (C), using the same FISH probes.

anemia, ALS- and FTD-like symptoms (170,171), reviewed (59). In such cases these presentations were reversed upon B12 supplementation—indicating that chromosomal instability was induced by folate-stress. Somatic GGGGCC repeat instability, FRA9A fragility and global increase of SCEs depend upon *C9orf72* expansion and are folate-sensitive and can occur in cells from presymptomatic *C9orf72*Exp individuals. *C9orf72*Exp carriers, in folate-deficient states, may be predisposed to repeat instability, FRA9A fragility and chromosomal instability, which if exacerbated over time may impact gene dysregulation, altering the susceptibility of phenotypic variations amongst *C9orf72*Exp carriers. Fragile sites and SCEs can be induced in the blood and myeloid cells by lifestyle choices, including cigarette smoking, alcohol consumption and diet (59,172–176). Tobacco and alcohol consumption by presymptomatic *C9orf72*Exp carriers affected disease age-of-onset (40). Various clinically used agents (177), including some considered for use in ALS/FTD, *C9orf72*Exp (178) and fragile X syndrome (179), like phenytoin or decitabine can induce fragile sites (59,180), induce SCEs (181,182) and modify chromosome condensation (183,184). Age-dependent ongoing repeat expansions in the brain have been suggested as a contributor to disease (26,70,185,186) and could be folate sensitive. Additionally, CpG-methylation of *C9orf72*Exp (185,187) and acceleration of genome-specific DNA methylation age (epigenetic clock) are modifiers of disease onset and progression in *C9orf72*Exp carriers (188,189). Chromatin compaction of *C9orf72*Exp is sensitive to the degree of expansion and CpG-methylation (Figure 5). Efforts to prophylactically slow the epigenetic clock are a central focus (190–192). The *C9orf72* expansion was recently reported to be bound by the chromatin remodeler DAXX (193). Coincidentally, DAXX, is known to associate with satellite and telomere repeats and its downregulation led to a global increase in MNase sensitivity (194–196). Environmental contributions to *C9orf72*Exp diseases must be considered.

Various genetic, molecular and environmental aspects have been demonstrated to modify disease presentation in *C9orf72*Exp carriers (3,4,7,8,40,42,45,197–204). The 90-year-old male *C9orf72*Exp carrier presented herein (Figure 5) is likely to be truly asymptomatic, as a long presymptomatic phase with evident degeneration often detected decades before ALS or FTD symptom manifestation (205,206), pathology that was not present in his brain (70). Clinical differences between the truly asymptomatic father and symptomatic daughter studied herein could not be explained by either genetic modifiers (*TMEM106B*, *ATXN2* and Finnish haplotype), both expressed similar burdens of p62 inclusions, similar burdens of sense and antisense RNA foci, similar burdens of all five types of RAN-peptides (GA > GP > GR > PA/PR, except for the cerebellum, which showed more RAN-peptide inclusions (~7-fold) and sense RNA foci (~2-fold) in the asymptomatic father compared to the ALS/FTD-affected daughter) (29,70) (summarized in Supplementary Table S2). Also, neither lifestyle choices, life events, nor autoimmunity, could explain their phenotypic differences (29,70) (Supplementary Table S2). However, compared to the daughter, in the brain the father showed extreme repeat length mosaicism (13–3500 repeats) (Figure 5D), with increased MNase accessibility of shorter expansions, increased *C9orf72* expression (mRNA and C9ORF72-long, but not C9ORF72-short protein) (29,70), increased TDP-43 inclusions (29,70) and an epigenetic age ~9 years younger than his chronologic

age (the daughter was 3 years older) (70,188) (summarized in Supplementary Table S2). Thus, these somatic variations deserve further attention in pre-, asymptomatic and symptomatic *C9orf72*Exp carriers.

FRA9A as a DNA source to activate the DDR and IFN pathways

Both a spontaneous activated DDR (15–25) and a hyperactivated IFN cGAS-STING-associated immune response occur in *C9orf72*Exp patient cells and brains (4,12–14). The source of the damaged DNA or DNA-immunostimulant to activate either DDR or IFN response is unknown. DDR in cells and brains of *C9orf72*Exp, evident as increased γ -H2AX, phosphorylated-ATM, cleaved Poly(ADP-ribose) polymerase-1 (PARP-1) and 53BP1, is coincident with DSBs (22–24). We reveal that DSBs arise at *C9orf72*Exp via heightened FRA9A fragility, broken/rearranged Chr9s, increased genome-wide SCEs, increased MN and Chr9-containing MN. The increased C9ORF72 protein levels in multiple tissues of the asymptomatic father shown to have massive mosaic somatic expansions (Figure 5F and Supplementary Table S2; (29,70)) may suppress an autoimmune response by increasing STING levels. Models of the *C9orf72*Exp-linked DDR activation involve RAN-peptide induced p53-target gene activation, inhibition or mislocalization of the DSB DNA repair proteins ATM, 53BP1, TDP-43, FUS, Ku80 and PARP-1 (15–25). Other non-RAN-peptide DDR paths have received little attention.

The unusual >33kb of compact chromatin at FRA9A's core fragility zone (Figure 5A) could be susceptible to DSBs, which would contribute to DDR activation. Supporting this possibility is that experimentally-induced locus-specific compacted chromatin of an artificial ~10 kb stretch of ~250 tandem arrays of LacO, which becomes a fragile site, has been demonstrated to activate a DDR in the absence of damage (207–210). A contribution of FRA9A fragility to DDR can act in parallel to RAN-peptide induced DDR (23,24). Disruption of higher-order chromosomal organization may also contribute to DDR and IFN responses. Long-range chromosomal interactions involving 9p21 are activated in the inflammatory response. All IFN genes at 9p21 are transcriptionally inactive until immunostimulated by viral infection or cytosolic self-DNAs, whereupon dramatic chromatin (211) and multiple intra-9p21, inter-arm (9p21-9q34.2), and inter-chromosomal (9p21-4p14 and 9p21-18q21.1) interactions arise to activate IFN cluster expression and inflammation (47,212). Reduced levels of the C9ORF72 protein in *C9orf72*Exp patients, being unable to suppress STING, leads to a sustained hyperactivation of IFN in brains (213). Upon FRA9A breakage the *C9orf72*Exp-Chr9 activates DDR and is then sequestered to MN whose contents can be released to the cytosol to activate IFN through cGAS-STING, and this sequestration may disrupt other inter- and intra-Chr9 interactions (214). That disruption of intra-/inter-chromosomal associations can drive DDR and IFN cascades is supported by the experimental disruption of such interactions leading to chromosome sequestration to MN (215,216). CGG expansions at *FMR1*, the cause of FRAXA, disrupt intra- and inter-chromosome interactions (217). The 2-fold increase in global SCEs in *C9orf72*Exp cells we observe may contribute to DDR and MN. MN enriched with the DSB repair protein, TDP-43, have been detected in brains of ALS patients (218). Our suggestion that DNA damage induced by FRA9A fragility can serve as a

DNA-immunostimulant in the CNS is consistent with reports of *in vivo* DNA damage by ATM-deficiency or brain trauma that activates an *IFN* response in motor neurons (219–221). Our working model that the *C9orf72Exp* acts as a chromatin compacted FSFS, is an inducer of DNA damage at many locations including on Chr9 and is suited to non-cycling neurons.

We suggest that the cytoplasmic release of DNA from FRA9A-enhanced MN, may further tip the balance by exacerbating the stimulation of the aberrantly hyperactive cGAS-STING initiated *IFN* expression in *C9orf72Exp* carriers (4,13,14), which may explain the co-morbid partially-penetrant autoimmunity (1–6). FRA9A broken-Chr9s and increased global SCEs might also further exacerbate the DDR cascade, as DNA-immunostimulation enhances sense and antisense transcription from *C9orf72* (42) whose RAN-peptide products would feedback upon the DDR by suppressing DSB DNA repair proteins ATM, p53, TDP-43, FUS, Ku80 and PARP-1 (15–25). The neuroinflammatory and autoimmune phenotypes of *C9orf72Exp* carriers is complex (14), and the effects of either FRA9A altered chromatin or MNs containing broken Chr9s upon the *IFN* response is unknown.

FRA9A chromosomal instability, mosaic somatic mutations and 9p21-associated diseases

A reasonable prediction from our findings is that the *C9orf72*/FRA9A fragile site may, like other fragile sites, predispose to mosaic deletions, duplications or rearrangements resulting in altered expression of genes on 9p21 or throughout Chr9. Such mosaic chromosomal variations may vary between tissues, accumulate with age, and lead to phenotypic variability. In the case of *FMR1*/FRAXA, phenotypic variability can arise through mosaic genetic or chromosomal instability (deletions, duplications and rearrangements) extending beyond the *FMR1* CGG-repeat, as revealed through decades of isolated case reports (59). Similar phenomena may arise at the mutant *C9orf72*, as suggested by our observation of truncated-Chr9s broken at *C9orf72*, acentric-Chr9s, chromosomal instability of the *C9orf72Exp* allele and heightened levels of genome-wide SCEs. Detection of somatic mosaic levels of chromosomal instability will likely require more focused studies. For example, the dramatic Chr9 rearrangements, evident by FISH in every metaphase of the ALS/*C9orf72Exp* line P8, escaped detection by repeat-primed PCR and by Southern blot assessment of the repeat size (compare Figure 3B with Figure 6F). Indeed, mosaic mutations at various loci (reviewed in (222–224)) including *FMR1* (225–230) required focused attention. Mosaic mutations may be confined to specific cell types, as recently revealed for Purkinje cells with large somatic CAG-expansions, amongst stable tracts in the cerebellum of Huntington's disease patients (231,232). One might expect an increase in somatic mutation rates throughout the genome in *C9orf72Exp* patients, as the increased 2-fold global SCEs we observed may have a coincident increase in mutation rate, similar to the 10-fold increased mutation rates in BLM individuals who show a 10-fold increase of SCEs (131,132,136,137). *C9orf72Exp* cells from presymptomatic individuals show folate-sensitive repeat instability, FRA9A fragility, chromosomal instability, MNase-resistance, increased levels of MN/NBuds and global SCEs. Long-term display of these features may exacerbate disease-onset and affect penetrance. Our findings support that the *C9orf72Exp* patients may incur mosaic mutations at under-appreciated

levels, and recent findings support increased somatic mutations in brains and spinal cords of *C9orf72Exp* individuals (233, <https://www.biorxiv.org/content/10.1101/2023.11.30.569436v1>).

Knowledge gaps remain for FRA9A/*C9orf72Exp*. In particular, the co-occurrence of many diverse phenotypes in *C9orf72* expansion carriers is unclear. That FRA9A encompasses the *IFN* cluster, *CDKN2A*, *IFNk*, *LINGO2*, *TOPORS*, *APT*X, *DNAJA1* and *SMU1* genes, each independently associated with symptoms that can co-occur in *C9orf72Exp* carriers, provide new insights into the possible involvement of chromosomal instability (Figure 1). An increase in ALS occurring in cancer survivors, particularly melanoma, has been repeatedly reported (7,234–238). While a correlation of *C9orf72Exp* in cancer predisposition has not been studied in large populations, *C9orf72Exp* carriers have a significantly higher risk of melanoma (7). *C9orf72Exp* carriers may succumb to cancer prior to onset or awareness of ALS. That both *CDKN2A* and the *IFN* gene cluster, frequently deleted in melanoma, are encompassed in FRA9A's fragility zone introduces the possible involvement of *C9orf72Exp*. Mosaic somatic mutations that extend beyond the *C9orf72* repeat may affect expression of genes encompassed by FRA9A or beyond. Thus, revisiting the *C9orf72*/9p21 locus with the awareness that it is, and can share the attributes of, a chromosomal fragile site should provide key insights into the genotype–phenotype relationships for the many and varied presentations associated with the 9p21 region.

Inclusion and ethics statement

All collaborators of this study who have fulfilled the criteria for authorship required by *NAR Molecular Medicine* and Oxford University Press journals are included as authors. Each author's contribution is detailed in the Author Contributions list. Expectations for collaborators were agreed upon ahead of the study's initiation, and authorship placement was agreed upon by each collaborator. This study was conducted in collaboration with researchers and physicians from distinct cultural, ethnic and racial backgrounds. The findings of this study apply to members of the population globally, as well as locally in the regions where patient recruitment occurred. The research does not result in stigmatization, incrimination, discrimination or personal risk to participants who provided samples. Local and regional research publications relevant to our study was considered and included in our bibliography.

The Hospital for Sick Children Research Ethics Board oversight and approval for the herein study was obtained. REB for human tissue, cell and animal studies: #1000056560.

Data availability

Datasets generated during the current study supporting its findings have been deposited or made available as indicated: RNASeq gene expression data—available on Gene Expression Omnibus (GEO), accession GSE262674. Whole genome sequencing data for the der-Chr9 (P8) sample is available in the European Genome-Phenome Archive (EGA) upon approval by the Data Access Committee. Correspondence and requests for materials should be addressed to Dr Christopher E. Pearson (mail to: cepearson.sickkids@gmail.com). Mouse models presented in this study are commercially available from Jackson Laboratories (FVB/NJ-Tg(*C9orf72*)500Lpwr/J).

Supplementary data

Supplementary Data are available at NARMME Online.

Acknowledgements

This study is dedicated to the memory of Dr Stephen T. Warren (1953–2021), a pioneer and advocate of Fragile X syndrome, a mentor and friend. This study is also dedicated to Robert K. Ranum, a joyful, persevering individual, and friend. We thank Robert H. Brown for providing a YAC-C9orf72 clone, John Volpe, Shamima Keka Islam for counting micronuclei, Lazar Joksimovic and Raymond Wong for his expertise in the preparation of metaphase spreads. We thank Olivia Beck and Lieve Wiericx for sharing their expertise in cytogenetic fragile site recognition and Edwin Reyniers and Stephen W. Scherer, Jeff MacDonald, Mehdi Zarrei, Mehdi Layeghifard and Bhooma Thiruvahindrapuram for help with the der-Chr9 data, and Michael Fenech for support regarding micronuclei, NBuds and NBlebs.

Author contributions: Conceptualization: C.E.P. and R.F.K.; Figure 1: C.E.P.; Figure 2: M.L., M.D.W. and C.E.P.; Figure 3: M.M., M.H.M.S., C.E.P., P.A.D., G.A.R., E.K. and M.Z.; Figure 4: M.M., I.v.d.W., S.S., R.F.K. and C.E.P.; Figure 5: M.H.M.S., T.K.P. and C.E.P. (sample collection by L.Z., J.K., A.A., P.M.c.G., P.M.c.K. and J.R.); Figure 6: M.M.*, M.H.M.S., N.S., S.L., K.Y., M.M.†, M.K., R.K.C.Y., P.M.c.K., J.R., L.S., M.S.S. and C.E.P.; Figure 7: N.S. and B.M. (training by M.M.*, M.H.M.S. and T.K.P.); Table 1: M.M.*, M.K. and C.E.P.; Figure S1: M.L., M.D.W. and C.E.P.; Supplementary Figure S2: M.M.*, M.Z., E.R. and M.H.M.S.; Supplementary Figure S3: M.M.*, I.v.d.W., S.S. and R.F.K.; Supplementary Figure S4: M.H.M.S.; Supplementary Figure S5: M.M.*; Supplementary Figure S6: M.M.*, M.M.†, S.L., N.S., K.Y., M.H.M.S. and C.E.P.; Supplementary Figure S7: T.A., E.A.P. and C.H.F.; Supplementary Figure S8: R.K.C.Y., R.F.K., M.M.* and L.S.; Supplementary Figure S9: N.S.; Supplementary Figure S10: B.M. (training by M.M.*); Supplementary Table S1: M.H.M.S.; Supplementary Table S2: L.Z., J.K., A.A., P.M.c.G., P.M.c.K., J.R. and C.E.P.; Supplementary Table S3: L.S., M.K., P.M.c.K., R.K.C.Y., J.R. and C.E.P.; Supplementary Table S4: M.K. and R.K.C.Y.; BAC DNA for patient C9orf72 provided by C.J., P.J.de.J.; ALS patient cells provided by P.A.D. and G.A.R.; Autopsy tissues prepared by L.Z., P.M.K. and J.R.; Intellectual input and experimental design: C.E.P., R.F.K., E.C., R.W., M.D.W., M.S.S. and E.R.; Supervision: C.E.P. and R.F.K.; Writing—original draft: MM*, CEP; Writing—review and editing: C.E.P., M.H.M.S., N.S., M.S.S. and M.M.†. All authors provided feedback on the manuscript; M.M.* = Mila Mirceta; M.M.† = Mohiuddin Mohiuddin.

Funding

ALS Canada-Brain Canada 2020 Discovery Grant [HSC0005599 to C.E.P., E.R., G.A.R.]; ALS Canada Doctoral Research Award 2016 [to M.H.M.S.]; Weston Family Foundation [TR202268 to C.E.P.]; W. Garfield Weston Foundation [CNV0001757 to C.E.P.]; Natural Sciences and Engineering Research Council of Canada (NSERC) [RGPIN-2019-07014 to M.D.W.], National Institutes of Health [GM122880 and GM144215 to C.H.F. and NS048843 to M.S.S.]; Muscular Dystrophy Association Development Grant [MDA546770

to L.S.], National Natural Science Foundation of China [82071430 to M.Z., E.R.]; James Hunter and Family ALS Initiative (to J.R., E.R.); Canadian Consortium on Neurodegeneration in Aging (to G.A.R., E.R.); ALS Association Milton Safenowitz Fellowship and ALS Double Play Christopher Chiu Fellowship [P.M.M.]; ALS Society of Canada Project Grant [to J.R.], ERA-LEARN (E-Rare-3/Canadian Institute for Health Research) grant (063-REPETOMICS) [J.R.].

Conflict of interest statement

M.S.S. is a Scientific Advisory Board member of Skyhawk Therapeutics and Tacit Therapeutics. For all other authors, no conflict declared.

References

- Atanasio,A., Decman,V., White,D., Ramos,M., Ikiz,B., Lee,H.-C., Siao,C.-J., Brydges,S., LaRosa,E., Bai,Y., *et al.* (2016) C9orf72 ablation causes immune dysregulation characterized by leukocyte expansion, autoantibody production, and glomerulonephropathy in mice. *Sci. Rep.*, **6**, 23204.
- Breevoort,S., Gibson,S., Figueroa,K., Bromberg,M. and Pulst,S. (2022) Expanding clinical spectrum of C9ORF72-related disorders and promising therapeutic strategies: a review. *Neurol. Genet.*, **8**, e670.
- Fredi,M., Cavazzana,I., Biasiotto,G., Filosto,M., Padovani,A., Monti,E., Tincani,A., Franceschini,F. and Zanella,I. (2019) C9orf72 intermediate alleles in patients with amyotrophic lateral sclerosis, systemic lupus erythematosus, and rheumatoid arthritis. *Neuromol. Med.*, **21**, 150–159.
- McCauley,M.E., O'Rourke,J.G., Yáñez,A., Markman,J.L., Ho,R., Wang,X., Chen,S., Lall,D., Jin,M., Muhammad,A.K.M.G., *et al.* (2020) C9orf72 in myeloid cells suppresses STING-induced inflammation. *Nature*, **585**, 96–101.
- Miller,Z.A., Sturm,V.E., Camsari,G.B., Karydas,A., Yokoyama,J.S., Grinberg,L.T., Boxer,A.L., Rosen,H.J., Rankin,K.P., Gorno-Tempini,M.L., *et al.* (2016) Increased prevalence of autoimmune disease within C9 and FTD/MND cohorts: completing the picture. *Neurol. Neuroimmunol. Neuroinflamm.*, **3**, e301.
- van der Ende,E.L., Jackson,J.L., White,A., Seelaar,H., van Blitterswijk,M. and Van Swieten,J.C. (2021) Unravelling the clinical spectrum and the role of repeat length in C9ORF72 repeat expansions. *J. Neurol. Neurosurg. Psychiatry*, **92**, 502–509.
- Tábuas-Pereira,M., Almendra,L., Almeida,M.R., Durães,J., Pinho,A., Matos,A., Negrão,L., Geraldo,A. and Santana,I. (2019) Increased risk of melanoma in C9ORF72 repeat expansion carriers: a case-control study. *Muscle Nerve*, **59**, 362–365.
- Chiò,A., Mazzini,L., D'Alfonso,S., Corrado,L., Canosa,A., Moglia,C., Manera,U., Bersano,E., Brunetti,M., Barberis,M., *et al.* (2018) The multistep hypothesis of ALS revisited: the role of genetic mutations. *Neurology*, **91**, e635–e642.
- Van Wijk,I.F., Van Eijk,R.P.A., Van Boxmeer,L., Westeneng,H.-J., Van Es,M.A., Van Rheenen,W., Van Den Berg,L.H., Eijkemans,M.J.C. and Veldink,J.H. (2024) Assessment of risk of ALS conferred by the GGGGCC hexanucleotide repeat expansion in C9orf72 among first-degree relatives of patients with ALS carrying the repeat expansion. *Amyotroph. Lateral Scler. Frontotemporal Degener.*, **25**, 188–196.
- Waite,A.J., Bäumer,D., East,S., Neal,J., Morris,H.R., Ansorge,O. and Blake,D.J. (2014) Reduced C9orf72 protein levels in frontal cortex of amyotrophic lateral sclerosis and frontotemporal degeneration brain with the C9ORF72 hexanucleotide repeat expansion. *Neurobiol. Aging*, **35**, 1779.e5–e1779.

11. Xiao,S., MacNair,L., McLean,J., McGoldrick,P., McKeever,P., Soleimani,S., Keith,J., Zinman,L., Rogaeva,E. and Robertson,J. (2016) C9orf72 isoforms in amyotrophic lateral sclerosis and frontotemporal lobar degeneration. *Brain Res.*, **1647**, 43–49.
12. Marques,C., Held,A., Dorfman,K., Sung,J., Song,C., Kavuturu,A.S., Aguilar,C., Russo,T., Oakley,D.H., Albers,M.W., *et al.* (2024) Neuronal STING activation in amyotrophic lateral sclerosis and frontotemporal dementia. *Acta Neuropathol.*, **147**, 56.
13. Pang,W. and Hu,F. (2023) C9ORF72 suppresses JAK-STAT mediated inflammation. *Iscience*, **26**, 106579.
14. Masrori,P., Beckers,J., Gossye,H. and Van Damme,P. (2022) The role of inflammation in neurodegeneration: novel insights into the role of the immune system in C9orf72 HRE-mediated ALS/FTD. *Mol. Neurodegener.*, **17**, 22.
15. Wang,Y., Liu,L., Chen,H., Yang,Y., Mu,C., Ren,H., Liu,Y., Yu,L., Fang,Q., Wang,G., *et al.* (2023) Disrupted phase behavior of FUS underlies poly-PR-induced DNA damage in amyotrophic lateral sclerosis. *Hum. Mol. Genet.*, **33**, 64–77.
16. Braems,E., Bercier,V., Van Schoor,E., Heeren,K., Beckers,J., Fumagalli,L., Dedeene,L., Moisse,M., Geudens,I., Hersmus,N., *et al.* (2022) HNRNPk alleviates RNA toxicity by counteracting DNA damage in C9orf72 ALS. *Acta Neuropathol.*, **144**, 465–488.
17. Konopka,A. and Atkin,J.D. (2022) DNA damage, defective DNA repair, and neurodegeneration in amyotrophic lateral sclerosis. *Front. Aging Neurosci.*, **14**, 786420.
18. Maor-Nof,M., Shipony,Z., Lopez-Gonzalez,R., Nakayama,L., Zhang,Y.-J., Couthouis,J., Blum,J.A., Castruita,P.A., Linares,G.R., Ruan,K., *et al.* (2021) p53 is a central regulator driving neurodegeneration caused by C9orf72 poly(PR). *Cell*, **184**, 689–708.
19. Andrade,N.S., Ramic,M., Esanov,R., Liu,W., Rybin,M.J., Gaidosh,G., Abdallah,A., Del’Olio,S., Huff,T.C., Chee,N.T., *et al.* (2020) Dipeptide repeat proteins inhibit homology-directed DNA double strand break repair in C9ORF72 ALS/FTD. *Mol. Neurodegener.*, **15**, 13.
20. Nihei,Y., Mori,K., Werner,G., Arzberger,T., Zhou,Q., Khosravi,B., Japtok,J., Hermann,A., Sommacal,A., Weber,M., *et al.* (2020) Poly-glycine-alanine exacerbates C9orf72 repeat expansion-mediated DNA damage via sequestration of phosphorylated ATM and loss of nuclear hnRNPA3. *Acta Neuropathol.*, **139**, 99–118.
21. Lopez-Gonzalez,R., Yang,D., Pribadi,M., Kim,T.S., Krishnan,G., Choi,S.Y., Lee,S., Coppola,G. and Gao,F.-B. (2019) Partial inhibition of the overactivated Ku80-dependent DNA repair pathway rescues neurodegeneration in C9ORF72-ALS/FTD. *Proc. Natl Acad. Sci. U.S.A.*, **116**, 9628–9633.
22. Konopka,A. and Atkin,J.D. (2018) The emerging role of DNA damage in the pathogenesis of the C9orf72 repeat expansion in amyotrophic lateral sclerosis. *Int. J. Mol. Sci.*, **19**, E3137.
23. Walker,C., Herranz-Martin,S., Karyka,E., Liao,C., Lewis,K., Elsayed,W., Lukashchuk,V., Chiang,S.-C., Ray,S., Mulcahy,P.J., *et al.* (2017) C9orf72 expansion disrupts ATM-mediated chromosomal break repair. *Nat. Neurosci.*, **20**, 1225–1235.
24. Farg,M.A., Konopka,A., Soo,K.Y., Ito,D. and Atkin,J.D. (2017) The DNA damage response (DDR) is induced by the C9orf72 repeat expansion in amyotrophic lateral sclerosis. *Hum. Mol. Genet.*, **26**, 2882–2896.
25. Lopez-Gonzalez,R., Lu,Y., Gendron,T.F., Karydas,A., Tran,H., Yang,D., Petrucelli,L., Miller,B.L., Almeida,S. and Gao,F.-B. (2016) Poly(GR) in C9ORF72-related ALS/FTD compromises mitochondrial function and increases oxidative stress and DNA damage in iPSC-derived motor neurons. *Neuron*, **92**, 383–391.
26. van Blitterswijk,M., DeJesus-Hernandez,M., Niemantsverdriet,E., Murray,M.E., Heckman,M.G., Diehl,N.N., Brown,P.H., Baker,M.C., Finch,N.A., Bauer,P.O., *et al.* (2013) Association between repeat sizes and clinical and pathological characteristics in carriers of C9ORF72 repeat expansions (Xpansize-72): A cross-sectional cohort study. *Lancet Neurol.*, **12**, 978–988.
27. Nordin,A., Akimoto,C., Wuolikainen,A., Alstermark,H., Jonsson,P., Birve,A., Marklund,S.L., Graffmo,K.S., Forsberg,K., Brännström,T., *et al.* (2015) Extensive size variability of the GGGGCC expansion in C9orf72 in both neuronal and non-neuronal tissues in 18 patients with ALS or FTD. *Hum. Mol. Genet.*, **24**, 3133–3142.
28. Akimoto,C., Volk,A.E., van Blitterswijk,M., Van den Broeck,M., Leblond,C.S., Lumbroso,S., Camu,W., Neitzel,B., Onodera,O., van Rheenen,W., *et al.* (2014) A blinded international study on the reliability of genetic testing for GGGGCC-repeat expansions in C9orf72 reveals marked differences in results among 14 laboratories. *J. Med. Genet.*, **51**, 419–424.
29. Xi,Z., van Blitterswijk,M., Zhang,M., McGoldrick,P., McLean,J.R., Yunusova,Y., Knock,E., Moreno,D., Sato,C., McKeever,P.M., *et al.* (2015) Jump from pre-mutation to pathologic expansion in C9orf72. *Am. J. Hum. Genet.*, **96**, 962–970.
30. Xi,Z., Yunusova,Y., van Blitterswijk,M., Dib,S., Ghani,M., Moreno,D., Sato,C., Liang,Y., Singleton,A., Robertson,J., *et al.* (2014) Identical twins with the C9orf72 repeat expansion are discordant for ALS. *Neurology*, **83**, 1476–1478.
31. Sattler,R., Traynor,B.J., Robertson,J., Van Den Bosch,L., Barmada,S.J., Svendsen,C.N., Disney,M.D., Gendron,T.F., Wong,P.C., Turner,M.R., *et al.* (2023) Roadmap for C9ORF72 in frontotemporal dementia and amyotrophic lateral sclerosis: report on the C9ORF72 FTD/ALS summit. *Neurol. Ther.*, **12**, 1821–1843.
32. Cammack,A.J., Balendra,R. and Isaacs,A.M. (2024) Failure of C9orf72 sense repeat-targeting antisense oligonucleotides: lessons learned and the path forward. *Brain*, **147**, 2607–2609.
33. Petri,S. (2024) Targeting C9orf72 in people with ALS. *Lancet Neurol.*, **23**, 850–852.
34. van den Berg,L.H., Rothstein,J.D., Shaw,P.J., Babu,S., Benatar,M., Buccelli,R.C., Genge,A., Glass,J.D., Hardiman,O., Libri,V., *et al.* (2024) Safety, tolerability, and pharmacokinetics of antisense oligonucleotide BIIB078 in adults with C9orf72-associated amyotrophic lateral sclerosis: a phase 1, randomised, double blinded, placebo-controlled, multiple ascending dose study. *Lancet Neurol.*, **23**, 901–912.
35. Wave Life Sciences Announces Topline Results from Phase 1b/2a FOCUS-C9 Study of WVE-004 for C9orf72-associated Amyotrophic Lateral Sclerosis and Frontotemporal Dementia - Wave Life Sciences. <https://www.neurologylive.com/view/wave-life-sciences-discontinues-c9orf72-als-frontotemporal-dementia-agent-wve-004-after-disappointing-phase-1b-2a-findings>, (25 November 2024, date last accessed).
36. Tran,H., Moazami,M.P., Yang,H., McKenna-Yasek,D., Douthwright,C.L., Pinto,C., Metterville,J., Shin,M., Sanil,N., Dooley,C., *et al.* (2022) Suppression of mutant C9orf72 expression by a potent mixed backbone antisense oligonucleotide. *Nat. Med.*, **28**, 117–124.
37. Saracino,D. and Le Ber,J. (2022) How can we define the presymptomatic C9orf72 disease in 2022? An overview on the current definitions of preclinical and prodromal phases. *Rev. Neurol. (Paris)*, **178**, 426–436.
38. Saracino,D. and Le Ber,J. (2021) Clinical update on C9orf72: frontotemporal dementia, amyotrophic lateral sclerosis, and beyond. *Adv. Exp. Med. Biol.*, **1281**, 67–76.
39. Mandrioli,J., Zucchi,E., Martinelli,I., Van der Most,L., Gianferrari,G., Moglia,C., Manera,U., Solero,L., Vasta,R., Canosa,A., *et al.* (2023) Factors predicting disease progression in C9ORF72 ALS patients. *J. Neurol.*, **270**, 877–890.
40. Westeneng,H.-J., van Veenhuijzen,K., van der Spek,R.A., Peters,S., Visser,A.E., van Rheenen,W., Veldink,J.H. and van den Berg,L.H. (2021) Associations between lifestyle and amyotrophic lateral sclerosis stratified by C9orf72 genotype: a longitudinal,

- population-based, case-control study. *Lancet Neurol.*, **20**, 373–384.
41. Querin, G., Biferi, M.G. and Pradat, P.-F. (2022) Biomarkers for C9orf7-ALS in symptomatic and pre-symptomatic patients: state-of-the-art in the new era of clinical trials. *J. Neuromuscul. Dis.*, **9**, 25–37.
 42. Rizzu, P., Blauwendraat, C., Heetveld, S., Lynes, E.M., Castillo-Lizardo, M., Dhingra, A., Pyz, E., Hobert, M., Synofzik, M., Simón-Sánchez, J., *et al.* (2016) C9orf72 is differentially expressed in the central nervous system and myeloid cells and consistently reduced in C9orf72, MAPT and GRN mutation carriers. *Acta Neuropathol. Commun.*, **4**, 37.
 43. Niblock, M., Smith, B.N., Lee, Y.-B., Sardone, V., Topp, S., Troakes, C., Al-Sarraj, S., Leblond, C.S., Dion, P.A., Rouleau, G.A., *et al.* (2016) Retention of hexanucleotide repeat-containing intron in C9orf72 mRNA: implications for the pathogenesis of ALS/FTD. *Acta Neuropathol. Commun.*, **4**, 18.
 44. Sznajder, Ł., Thomas, J.D., Carrell, E.M., Reid, T., McFarland, K.N., Cleary, J.D., Oliveira, R., Nutter, C.A., Bhatt, K., Sobczak, K., *et al.* (2018) Intron retention induced by microsatellite expansions as a disease biomarker. *Proc. Natl Acad. Sci. U.S.A.*, **115**, 4234–4239.
 45. Ben-Dor, I., Pacut, C., Nevo, Y., Feldman, E.L. and Reubinoff, B.E. (2021) Characterization of C9orf72 haplotypes to evaluate the effects of normal and pathological variations on its expression and splicing. *PLoS Genet.*, **17**, e1009445.
 46. Sarkar, M.K., Hile, G.A., Tsoi, L.C., Xing, X., Liu, J., Liang, Y., Berthier, C.C., Swindell, W.R., Patrick, M.T., Shao, S., *et al.* (2018) Photosensitivity and type I IFN responses in cutaneous lupus are driven by epidermal-derived interferon kappa. *Ann. Rheum. Dis.*, **77**, 1653–1664.
 47. Harismendy, O., Notani, D., Song, X., Rahim, N.G., Tanasa, B., Heintzman, N., Ren, B., Fu, X.-D., Topol, E.J., Rosenfeld, M.G., *et al.* (2011) 9p21 DNA variants associated with coronary artery disease impair interferon- γ signalling response. *Nature*, **470**, 264–268.
 48. Joung, J., Engreitz, J.M., Konermann, S., Abudayyeh, O.O., Verdine, V.K., Aguet, F., Gootenberg, J.S., Sanjana, N.E., Wright, J.B., Fulco, C.P., *et al.* (2017) Genome-scale activation screen identifies a lncRNA locus regulating a gene neighbourhood. *Nature*, **548**, 343–346.
 49. Ahel, I., Rass, U., El-Khamisy, S.F., Katyal, S., Clements, P.M., McKinnon, P.J., Caldecott, K.W. and West, S.C. (2006) The neurodegenerative disease protein aprataxin resolves abortive DNA ligation intermediates. *Nature*, **443**, 713–716.
 50. Lim, G., Karaskova, J., Beheshti, B., Vukovic, B., Bayani, J., Selvarajah, S., Watson, S.K., Lam, W.L., Zielenska, M. and Squire, J.A. (2005) An integrated mBAND and submegabase resolution tiling set (SMRT) CGH array analysis of focal amplification, microdeletions, and ladder structures consistent with breakage-fusion-bridge cycle events in osteosarcoma. *Genes Chromosomes Cancer*, **42**, 392–403.
 51. Fletcher, J.A., Gebhardt, M.C. and Kozakewich, H.P. (1994) Cytogenetic aberrations in osteosarcomas. Nonrandom deletions, rings, and double-minute chromosomes. *Cancer Genet. Cytogenet.*, **77**, 81–88.
 52. Giollant, M., Bertrand, S., Verrelle, P., Tchirkov, A., du Manoir, S., Ried, T., Mornex, F., Doré, J.F., Cremer, T. and Malet, P. (1996) Characterization of double minute chromosomes' DNA content in a human high grade astrocytoma cell line by using comparative genomic hybridization and fluorescence in situ hybridization. *Hum. Genet.*, **98**, 265–270.
 53. Satinover, D.L., Vance, G.H., Van Dyke, D.L. and Schwartz, S. (2001) Cytogenetic analysis and construction of a BAC contig across a common neocentromeric region from 9p. *Chromosoma*, **110**, 275–283.
 54. Jee, K.J., Kim, Y.T., Kim, K.R., Aalto, Y. and Knuutila, S. (2001) Amplification at 9p in cervical carcinoma by comparative genomic hybridization. *Anal. Cell. Pathol.*, **22**, 159–163.
 55. Sams, E.I., Ng, J.K., Tate, V., Claire Hou, Y.-C., Cao, Y., Antonacci-Fulton, L., Belhassan, K., Neidich, J., Mitra, R.D., Cole, F.S., *et al.* (2022) From karyotypes to precision genomics in 9p deletion and duplication syndromes. *HGG Adv.*, **3**, 100081.
 56. Shapiro, J.A. (2021) How chaotic is genome chaos? *Cancers (Basel)*, **13**, 1358.
 57. Bignell, G.R., Greenman, C.D., Davies, H., Butler, A.P., Edkins, S., Andrews, J.M., Buck, G., Chen, L., Beare, D., Latimer, C., *et al.* (2010) Signatures of mutation and selection in the cancer genome. *Nature*, **463**, 893–898.
 58. Sutherland, G.R., Jacky, P.B., Baker, E. and Manuel, A. (1983) Heritable fragile sites on human chromosomes. X. New folate-sensitive fragile sites: 6p23, 9p21, 9q32, and 11q23. *Am. J. Hum. Genet.*, **35**, 432–437.
 59. Mirceta, M., Shum, N., Schmidt, M.H.M. and Pearson, C.E. (2022) Fragile sites, chromosomal lesions, tandem repeats, and disease. *Front. Genet.*, **13**, 985975.
 60. Van Mossevelde, S., van der Zee, J., Cruts, M. and Van Broeckhoven, C. (2017) Relationship between C9orf72 repeat size and clinical phenotype. *Curr. Opin. Genet. Dev.*, **44**, 117–124.
 61. DeJesus-Hernandez, M., Mackenzie, I.R., Boeve, B.F., Boxer, A.L., Baker, M., Rutherford, N.J., Nicholson, A.M., Finch, N.A., Flynn, H., Adamson, J., *et al.* (2011) Expanded GGGGCC hexanucleotide repeat in noncoding region of C9orf72 causes chromosome 9p-linked FTD and ALS. *Neuron*, **72**, 245–256.
 62. Xi, Z., Zhang, M., Bruni, A.C., Maletta, R.G., Colao, R., Fratta, P., Polke, J.M., Sweeney, M.G., Mudanohwo, E., Nacmias, B., *et al.* (2015) The C9orf72 repeat expansion itself is methylated in ALS and FTL D patients. *Acta Neuropathol.*, **129**, 715–727.
 63. Sun, J.H., Zhou, L., Emerson, D.J., Phyto, S.A., Titus, K.R., Gong, W., Gilgenast, T.G., Beagan, J.A., Davidson, B.L., Tassone, F., *et al.* (2018) Disease-associated short tandem repeats co-localize with chromatin domain boundaries. *Cell*, **175**, 224–238.
 64. Xi, Z., Rainero, I., Rubino, E., Pinessi, L., Bruni, A.C., Maletta, R.G., Nacmias, B., Sorbi, S., Galimberti, D., Surace, E.I., *et al.* (2014) Hypermethylation of the CpG-island near the C9orf72 GC₂-repeat expansion in FTL D patients. *Hum. Mol. Genet.*, **23**, 5630–5637.
 65. Utani, K., Okamoto, A. and Shimizu, N. (2011) Generation of micronuclei during interphase by coupling between cytoplasmic membrane blebbing and nuclear budding. *PLoS One*, **6**, e27233.
 66. Fenech, M. (2007) Cytokinesis-block micronucleus cytome assay. *Nat. Protoc.*, **2**, 1084–1104.
 67. Migliore, L., Coppedè, F., Fenech, M. and Thomas, P. (2011) Association of micronucleus frequency with neurodegenerative diseases. *Mutagenesis*, **26**, 85–92.
 68. Fenech, M., Kirsch-Volders, M., Natarajan, A.T., Surrallés, J., Crott, J.W., Parry, J., Norppa, H., Eastmond, D.A., Tucker, J.D. and Thomas, P. (2011) Molecular mechanisms of micronucleus, nucleoplasmic bridge and nuclear bud formation in mammalian and human cells. *Mutagenesis*, **26**, 125–132.
 69. Polleys, E.J. and Freudenreich, C.H. (2018) Methods to study repeat fragility and instability in *Saccharomyces cerevisiae*. *Methods Mol. Biol.*, **1672**, 403–419.
 70. McGoldrick, P., Zhang, M., van Blitterswijk, M., Sato, C., Moreno, D., Xiao, S., Zhang, A.B., McKeever, P.M., Weichert, A., Schneider, R., *et al.* (2018) Unaffected mosaic C9orf72 case: RNA foci, dipeptide proteins, but upregulated C9orf72 expression. *Neurology*, **90**, e323–e331.
 71. Dingwall, C., Lomonosoff, G.P. and Laskey, R.A. (1981) High sequence specificity of micrococcal nuclease. *Nucleic Acids Res.*, **9**, 2659–2673.
 72. Hörz, W. and Altenburger, W. (1981) Sequence specific cleavage of DNA by micrococcal nuclease. *Nucleic Acids Res.*, **9**, 2643–2658.
 73. Bastepe, M. and Xin, W. (2015) Huntington disease: molecular diagnostics approach. *Curr. Protoc. Hum. Genet.*, **87**, 9.26.1–9.26.23.
 74. Nutter, C.A., Bubenik, J.L., Oliveira, R., Ivankovic, F., Sznajder, Ł., Kidd, B.M., Pinto, B.S., Otero, B.A., Carter, H.A., Vitriol, E.A., *et al.*

- (2019) Cell-type-specific dysregulation of RNA alternative splicing in short tandem repeat mouse knockin models of myotonic dystrophy. *Genes Dev.*, **33**, 1635–1640.
75. Love, M.I., Huber, W. and Anders, S. (2014) Moderated estimation of fold change and dispersion for RNA-seq data with DESeq2. *Genome Biol.*, **15**, 550.
 76. Patro, R., Duggal, G., Love, M.I., Irizarry, R.A. and Kingsford, C. (2017) Salmon provides fast and bias-aware quantification of transcript expression. *Nat. Methods*, **14**, 417–419.
 77. Semenov, M. (2021) Proliferative capacity of adult mouse brain. *Int. J. Mol. Sci.*, **22**, 3449.
 78. Bordiuk, O.L., Smith, K., Morin, P.J. and Semenov, M.V. (2014) Cell proliferation and neurogenesis in adult mouse brain. *PLoS One*, **9**, e111453.
 79. Lui, J.C. and Baron, J. (2011) Mechanisms limiting body growth in mammals. *Endocr. Rev.*, **32**, 422–440.
 80. Sanz, M.M., Jenkins, E.C., Brown, W.T., Davisson, M.T., Kevin, M.J., Roderick, T.H., Silverman, W.P. and Wisniewski, H.M. (1986) Mouse chromosome fragility. *Am. J. Med. Genet.*, **23**, 491–509.
 81. Angelosanto, F.A. (1995) Tissues other than bone marrow that can be used for cytogenetic analyses. *Environ. Mol. Mutagen.*, **25**, 338–343.
 82. Bayani, J. and Squire, J.A. (2004) Preparation of cytogenetic specimens from tissue samples. *Curr. Protoc. Cell Biol.*, **Chapter 22**(1), Unit 22.2.
 83. Krawczun, M.S., Lele, K.P., Jenkins, E.C. and Brown, W.T. (1986) Fragile X expression increased by low cell-culture density. *Am. J. Med. Genet.*, **23**, 467–473.
 84. Fonatsch, C. and Schwinger, E. (1983) Frequency of fragile X chromosomes, fra(X), in lymphocytes in relation to blood storage time and culture techniques. *Hum. Genet.*, **64**, 39–41.
 85. Brookwell, R., Daniel, A., Turner, G. and Fishburn, J. (1982) The fragile X(q27) form of X-linked mental retardation: FUDR as an inducing agent for fra(X)(q27) expression in lymphocytes, fibroblasts, and amniocytes. *Am. J. Med. Genet.*, **13**, 139–148.
 86. Daniel, A., Ekblom, L. and Phillips, S. (1984) Constitutive fragile sites 1p31, 3p14, 6q26, and 16q23 and their use as controls for false-negative results with the fragile(X). *Am. J. Med. Genet.*, **18**, 483–491.
 87. Reddy, K., Zamiri, B., Stanley, S.Y., Macgregor, R.B. and Pearson, C.E. (2013) The disease-associated r(GGGGCC)_n repeat from the C9orf72 gene forms tract length-dependent uni- and multimolecular RNA G-quadruplex structures. *J. Biol. Chem.*, **288**, 9860–9866.
 88. Zamiri, B., Mirceta, M., Bomsztyk, K., Macgregor, R.B. and Pearson, C.E. (2015) Quadruplex formation by both G-rich and C-rich DNA strands of the C9orf72 (GGGGCC)₈(GGCCCC)₈ repeat: effect of CpG methylation. *Nucleic Acids Res.*, **43**, 10055–10064.
 89. Fry, M. and Loeb, L.A. (1994) The fragile X syndrome d(CGG)_n nucleotide repeats form a stable tetrahelical structure. *Proc. Natl Acad. Sci. U.S.A.*, **91**, 4950–4954.
 90. Xi, Z., Zinman, L., Moreno, D., Schymick, J., Liang, Y., Sato, C., Zheng, Y., Ghani, M., Dib, S., Keith, J., et al. (2013) Hypermethylation of the CpG island near the G4C2 repeat in ALS with a C9orf72 expansion. *Am. J. Hum. Genet.*, **92**, 981–989.
 91. Jackson, J.L., Finch, N.A., Baker, M.C., Kachergus, J.M., DeJesus-Hernandez, M., Pereira, K., Christopher, E., Prudencio, M., Heckman, M.G., Thompson, E.A., et al. (2020) Elevated methylation levels, reduced expression levels, and frequent contractions in a clinical cohort of C9orf72 expansion carriers. *Mol. Neurodegen.*, **15**, 7.
 92. Xu, G.L., Bestor, T.H., Bourc'his, D., Hsieh, C.L., Tommerup, N., Bugge, M., Hulten, M., Qu, X., Russo, J.J. and Viegas-Péquignot, E. (1999) Chromosome instability and immunodeficiency syndrome caused by mutations in a DNA methyltransferase gene. *Nature*, **402**, 187–191.
 93. Hecht, F. and Sutherland, G.R. (1984) Detection of the fragile X chromosome and other fragile sites. *Clin. Genet.*, **26**, 301–303.
 94. Veenema, H., Beverstock, G.C., de Koning, T., Pearson, P.L. and van de Kamp, J.J. (1988) The fragile X-chromosome: an evaluation of the results in a routine cytogenetic laboratory in the period 1981–1986. *Clin. Genet.*, **33**, 410–417.
 95. Cantú, E.S. and Jacobs, P.A. (1984) Fragile (X) expression: relationship to the cell cycle. *Hum. Genet.*, **67**, 99–102.
 96. Yu, S., Mangelsdorf, M., Hewett, D., Hobson, L., Baker, E., Eyre, H.J., Lapsys, N., Le Paslier, D., Doggett, N.A., Sutherland, G.R., et al. (1997) Human chromosomal fragile site FRA16B is an amplified AT-rich minisatellite repeat. *Cell*, **88**, 367–374.
 97. Nancarrow, J.K., Kremer, E., Holman, K., Eyre, H., Doggett, N.A., Le Paslier, D., Callen, D.F., Sutherland, G.R. and Richards, R.I. (1994) Implications of FRA16A structure for the mechanism of chromosomal fragile site genesis. *Science*, **264**, 1938–1941.
 98. Bosco, N., Pelliccia, F. and Rocchi, A. (2010) Characterization of FRA7B, a human common fragile site mapped at the 7p chromosome terminal region. *Cancer Genet. Cytogenet.*, **202**, 47–52.
 99. Callahan, G., Denison, S.R., Phillips, L.A., Shridhar, V. and Smith, D.I. (2003) Characterization of the common fragile site FRA9E and its potential role in ovarian cancer. *Oncogene*, **22**, 590–601.
 100. Curatolo, A., Limongi, Z.M., Pelliccia, F. and Rocchi, A. (2007) Molecular characterization of the human common fragile site FRA1H. *Genes Chromosomes Cancer*, **46**, 487–493.
 101. Rozier, L., El-Achkar, E., Apiou, F. and Debatisse, M. (2004) Characterization of a conserved aphidicolin-sensitive common fragile site at human 4q22 and mouse 6C1: possible association with an inherited disease and cancer. *Oncogene*, **23**, 6872–6880.
 102. Becker, N.A., Thorland, E.C., Denison, S.R., Phillips, L.A. and Smith, D.I. (2002) Evidence that instability within the FRA3B region extends four megabases. *Oncogene*, **21**, 8713–8722.
 103. Fechter, A., Buettel, J., Kuehnel, E., Savelyeva, L. and Schwab, M. (2007) Common fragile site FRA11G and rare fragile site FRA11B at 11q23.3 encompass distinct genomic regions. *Genes Chromosomes Cancer*, **46**, 98–106.
 104. Hirst, M.C., Rack, K., Nakahori, Y., Roche, A., Bell, M.V., Flynn, G., Christadoulou, Z., MacKinnon, R.N., Francis, M. and Littler, A.J. (1991) A YAC contig across the fragile X site defines the region of fragility. *Nucleic Acids Res.*, **19**, 3283.
 105. Verkerk, A.J., Eussen, B.H., Van Hemel, J.O. and Oostra, B.A. (1992) Limited size of the fragile X site shown by fluorescence in situ hybridization. *Am. J. Med. Genet.*, **43**, 187–191.
 106. Hirst, M.C., Barnicoat, A., Flynn, G., Wang, Q., Daker, M., Buckle, V.J., Davies, K.E. and Bobrow, M. (1993) The identification of a third fragile site, FRAXE, in Xq27–q28 distal to both FRAXA and FRAXE. *Hum. Mol. Genet.*, **2**, 197–200.
 107. Ritchie, R.J., Knight, S.J., Hirst, M.C., Grewal, P.K., Bobrow, M., Cross, G.S. and Davies, K.E. (1994) The cloning of FRAXF: trinucleotide repeat expansion and methylation at a third fragile site in distal Xqter. *Hum. Mol. Genet.*, **3**, 2115–2121.
 108. Abruzzo, M.A., Hunt, P.A., Mayer, M., Jacobs, P.A., Wang, J.C. and Erbe, R.W. (1986) A comparison of fragile X expression in lymphocyte and lymphoblastoid cultures. *Am. J. Hum. Genet.*, **38**, 533–539.
 109. Sutherland, G.R., Baker, E. and Callen, D.F. (1988) A BrdU-enhanceable fragile site or viral modification site at 11q23.1 in lymphoblastoid cultures. *Cytogenet. Cell Genet.*, **47**, 201–203.
 110. Seki, N., Tsuji, H., Takahashi, E., Yamauchi, M., Saito, T., Hashimoto, T., Yamamoto, K. and Hori, T. (1992) Induction of a BrdU-enhanceable fragile site-like lesion and sister chromatid exchanges at 11q23.1 in EBV-transformed lymphoblastoid cell lines. *Cytogenet. Cell Genet.*, **61**, 95–98.
 111. Sutherland, G.R. and Baker, E. (2003) Forgotten fragile sites and related phenomena. *Cytogenet. Genome Res.*, **100**, 89–91.

112. Li, J.S.Z., Abbasi, A., Kim, D.H., Lippman, S.M., Alexandrov, L.B. and Cleveland, D.W. (2023) Chromosomal fragile site breakage by EBV-encoded EBNA1 at clustered repeats. *Nature*, **616**, 504–509.
113. Belzil, V.V., Bauer, P.O., Prudencio, M., Gendron, T.F., Stetler, C.T., Yan, I.K., Pregent, L., Daugherty, L., Baker, M.C., Rademakers, R., et al. (2013) Reduced C9orf72 gene expression in c9FTD/ALS is caused by histone trimethylation, an epigenetic event detectable in blood. *Acta Neuropathol.*, **126**, 895–905.
114. Cali, C.P., Patino, M., Tai, Y.K., Ho, W.Y., McLean, C.A., Morris, C.M., Seeley, W.W., Miller, B.L., Gaig, C., Vonsattel, J.P.G., et al. (2019) C9orf72 intermediate repeats are associated with corticobasal degeneration, increased C9orf72 expression and disruption of autophagy. *Acta Neuropathol.*, **138**, 795–811.
115. Tassone, F., Hagerman, R.J., Taylor, A.K., Gane, L.W., Godfrey, T.E. and Hagerman, P.J. (2000) Elevated Levels of FMR1 mRNA in Carrier Males: A New Mechanism of Involvement in the Fragile-X Syndrome. *Am. Hum. Genet.*, **66**, 6–15.
116. Eberhart, D.E. and Warren, S.T. (1996) Nuclease sensitivity of permeabilized cells confirms altered chromatin formation at the fragile X locus. *Somat. Cell Mol. Genet.*, **22**, 435–441.
117. Beverstock, G.C., Mol, A. and Wienhofer, E. (1985) Absence of significant autosomal lesions in Huntington's disease. *Ann. Hum. Genet.*, **49**, 283–290.
118. Krupina, K., Goginashvili, A. and Cleveland, D.W. (2021) Causes and consequences of micronuclei. *Curr. Opin. Cell Biol.*, **70**, 91–99.
119. Shimizu, N., Itoh, N., Utiyama, H. and Wahl, G.M. (1998) Selective entrapment of extrachromosomally amplified DNA by nuclear budding and micronucleation during S phase. *J. Cell Biol.*, **140**, 1307–1320.
120. Guttenbach, M. and Schmid, M. (1994) Exclusion of specific human chromosomes into micronuclei by 5-azacytidine treatment of lymphocyte cultures. *Exp. Cell Res.*, **211**, 127–132.
121. Bjerregaard, V.A., Garribba, L., McMurray, C.T., Hickson, I.D. and Liu, Y. (2018) Folate deficiency drives mitotic missegregation of the human FRAXA locus. *Proc. Natl Acad. Sci. U.S.A.*, **115**, 13003–13008.
122. Duncan, A.M. (1986) Enhanced sensitivity of lymphoblastoid cells from individuals carrying the mutation for the fragile X syndrome to the clastogenic effects of FUDR. *Mutat. Res.*, **173**, 201–205.
123. Shah, P., Wolf, K. and Lammerding, J. (2017) Bursting the bubble - nuclear envelope rupture as a path to genomic instability? *Trends Cell Biol.*, **27**, 546–555.
124. Srivastava, N., Nader, G.P., de, F., Williard, A., Rollin, R., Cuvelier, D., Lomakin, A. and Piel, M. (2021) Nuclear fragility, blaming the blebs. *Curr. Opin. Cell Biol.*, **70**, 100–108.
125. Stephens, A.D., Liu, P.Z., Banigan, E.J., Almossalha, L.M., Backman, V., Adam, S.A., Goldman, R.D. and Marko, J.F. (2018) Chromatin histone modifications and rigidity affect nuclear morphology independent of lamins. *Mol. Biol. Cell*, **29**, 220–233.
126. Bercht Pfleghaar, K., Taimen, P., Butin-Israeli, V., Shimi, T., Langer-Freitag, S., Markaki, Y., Goldman, A.E., Wehnert, M. and Goldman, R.D. (2015) Gene-rich chromosomal regions are preferentially localized in the lamin B deficient nuclear blebs of atypical progeria cells. *Nucleus*, **6**, 66–76.
127. Niedernhofer, L.J., Gurkar, A.U., Wang, Y., Vijg, J., Hoeijmakers, J.H.J. and Robbins, P.D. (2018) Nuclear genomic instability and aging. *Annu. Rev. Biochem.*, **87**, 295–322.
128. Fitchett, M. and Seabright, M. (1984) Deleted X chromosomes in patients with the fragile X syndrome. *J. Med. Genet.*, **21**, 373.
129. Verdyck, P., Berckmoes, V., De Vos, A., Verpoest, W., Liebaers, J., Bonduelle, M. and De Rycke, M. (2015) Chromosome fragility at FRAXA in human cleavage stage embryos at risk for fragile X syndrome. *Am. J. Med. Genet. A*, **167A**, 2306–2313.
130. Wenger, S.L., Hennessey, J.C. and Steele, M.W. (1987) Increased sister chromatid exchange frequency at Xq27 site in affected fragile X males. *Am. J. Med. Genet.*, **26**, 909–914.
131. van Wietmarschen, N., Merzouk, S., Halsema, N., Spierings, D.C.J., Guryev, V. and Lansdorp, P.M. (2018) BLM helicase suppresses recombination at G-quadruplex motifs in transcribed genes. *Nat. Commun.*, **9**, 271.
132. Chan, K.L., Palmal-Pallag, T., Ying, S. and Hickson, I.D. (2009) Replication stress induces sister-chromatid bridging at fragile site loci in mitosis. *Nat. Cell Biol.*, **11**, 753–760.
133. Chaganti, R.S., Schonberg, S. and German, J. (1974) A manyfold increase in sister chromatid exchanges in Bloom's syndrome lymphocytes. *Proc. Natl Acad. Sci. U.S.A.*, **71**, 4508–4512.
134. Cunniff, C., Bassetti, J.A. and Ellis, N.A. (2017) Bloom's syndrome: clinical spectrum, molecular pathogenesis, and cancer predisposition. *Mol. Syndromol.*, **8**, 4–23.
135. Gratia, M., Rodero, M.P., Conrad, C., Bou Samra, E., Maurin, M., Rice, G.I., Duffy, D., Revy, P., Petit, F., Dale, R.C., et al. (2019) Bloom syndrome protein restrains innate immune sensing of micronuclei by cGAS. *J. Exp. Med.*, **216**, 1199–1213.
136. Suzuki, T., Yasui, M. and Honma, M. (2016) Mutator phenotype and DNA double-strand break repair in BLM helicase-deficient human cells. *Mol. Cell Biol.*, **36**, 2877–2889.
137. Warren, S.T., Schultz, R.A., Chang, C.C., Wade, M.H. and Trosko, J.E. (1981) Elevated spontaneous mutation rate in Bloom syndrome fibroblasts. *Proc. Natl Acad. Sci. U.S.A.*, **78**, 3133–3137.
138. Wenger, S.L. (1995) Chemical induction of sister chromatid exchange at fragile sites. *Cancer Genet. Cytogenet.*, **85**, 72–74.
139. Kumar, J.V., Saraswathi, T., Ranganathan, K., Umadevi, K., Joshua, E. and Rooban, T. (2012) Sister chromatid exchanges in smokers and smokers with alcohol habit. *J. Oral Maxillofac. Pathol.*, **16**, 338–342.
140. Glover, T.W. and Stein, C.K. (1987) Induction of sister chromatid exchanges at common fragile sites. *Am. J. Hum. Genet.*, **41**, 882–890.
141. Fuster, C., Mirò, R., Templado, C., Barrios, L. and Egozcue, J. (1988) Can sister chromatid intercrossings be considered as prelesions? *Hum. Genet.*, **79**, 179–180.
142. Gaddini, L., Pelliccia, F., Limongi, M.Z. and Rocchi, A. (1995) Study of the relationships between common fragile sites, chromosome breakages and sister chromatid exchanges. *Mutagenesis*, **10**, 257–260.
143. Gregory, P., Wang, N. and Howard-Peebles, P.N. (1986) Analysis of sister chromatid exchanges in fra (X) individuals. *Am. J. Med. Genet.*, **23**, 563–566.
144. Branda, R.F., Arthur, D.C., Woods, W.G., Danzl, T.J. and King, R.A. (1984) Folate metabolism and chromosomal stability in the fragile X syndrome. *Am. J. Med.*, **77**, 602–611.
145. Suleimanova, D.G. and Kuleshov, N.P. (1987) [Spontaneous and induced chromosome instability in patients with fragile X syndrome]. *Genetika*, **23**, 504–509.
146. Schmid, M., Feichtinger, W. and Haaf, T. (1987) The fragile site (16)(q22). II. Sister chromatid exchanges. *Hum. Genet.*, **76**, 365–368.
147. Hirsch, B. (1991) Sister chromatid exchanges are preferentially induced at expressed and nonexpressed common fragile sites. *Hum. Genet.*, **87**, 302–306.
148. Lukusa, T., Meulepas, E., Fryns, J.P., Van den Berghe, H. and Cassiman, J.J. (1991) 'Spontaneous' FRA16B is a hot spot for sister chromatid exchanges. *Hum. Genet.*, **87**, 583–586.
149. Recalcati, M.P., Bellini, M., Norsa, L., Ballarati, L., Caselli, R., Russo, S., Larizza, L. and Giardino, D. (2012) Complex rearrangement involving 9p deletion and duplication in a syndromic patient: genotype/phenotype correlation and review of the literature. *Gene*, **502**, 40–45.
150. Korbel, J.O. and Campbell, P.J. (2013) Criteria for inference of chromothripsis in cancer genomes. *Cell*, **152**, 1226–1236.
151. Kinsella, M., Patel, A. and Bafna, V. (2014) The elusive evidence for chromothripsis. *Nucleic Acids Res.*, **42**, 8231–8242.
152. Krupina, K., Goginashvili, A. and Cleveland, D.W. (2024) Scrambling the genome in cancer: causes and consequences of

- complex chromosome rearrangements. *Nat. Rev. Genet.*, **25**, 196–210.
153. Zhang,C.-Z., Spektor,A., Cornils,H., Francis,J.M., Jackson,E.K., Liu,S., Meyerson,M. and Pellman,D. (2015) Chromothripsis from DNA damage in micronuclei. *Nature*, **522**, 179–184.
 154. Leibowitz,M.L., Papathanasiou,S., Doerfler,P.A., Blaine,L.J., Sun,L., Yao,Y., Zhang,C.-Z., Weiss,M.J. and Pellman,D. (2021) Chromothripsis as an on-target consequence of CRISPR-Cas9 genome editing. *Nat. Genet.*, **53**, 895–905.
 155. Urnov,F.D. (2021) CRISPR-Cas9 can cause chromothripsis. *Nat. Genet.*, **53**, 768–769.
 156. Pattamatta,A., Nguyen,L., Olafson,H.R., Scotti,M.M., Laboissonniere,L.A., Richardson,J., Berglund,J.A., Zu,T., Wang,E.T. and Ranum,L.P.W. (2021) Repeat length increases disease penetrance and severity in C9orf72 ALS/FTD BAC transgenic mice. *Hum. Mol. Genet.*, **29**, 3900–3918.
 157. Kähkönen,M., Tengström,C., Alitalo,T., Matilainen,R., Kaski,M. and Airaksinen,E. (1989) Population cytogenetics of folate-sensitive fragile sites. II. Autosomal rare fragile sites. *Hum. Genet.*, **82**, 3–8.
 158. Vasta,R., Chia,R., Traynor,B.J. and Chiò,A. (2022) Unraveling the complex interplay between genes, environment, and climate in ALS. *EBioMedicine*, **75**, 103795.
 159. Goncharova,P.S., Davydova,T.K., Popova,T.E., Novitsky,M.A., Petrova,M.M., Gavriljuk,O.A., Al-Zamil,M., Zhukova,N.G., Nasyrova,R.F. and Shnyder,N.A. (2021) Nutrient effects on motor neurons and the risk of amyotrophic lateral sclerosis. *Nutrients*, **13**, 3804.
 160. Cingam,S.R., Koshy,N., Veillon,D. and Peddi,P. (2017) Reversal of isolated 20q deletion with vitamin B12 replacement in a patient with pernicious anaemia. *BMJ Case Rep.*, **2017**, bcr2016218689.
 161. Wollman,M.R., Penschansky,L. and Shekhter-Levin,S. (1996) Transient 7q- in association with megaloblastic anemia due to dietary folate and vitamin B12 deficiency. *J. Pediatr. Hematol. Oncol.*, **18**, 162–165.
 162. Goh,K. (1981) Vitamin B12 deficiency in an 18p-patient. *Arch. Pathol. Lab. Med.*, **105**, 164.
 163. Parmentier,S., Meinel,J., Oelschlaegel,U., Mohr,B., Ehninger,G., Schaich,M. and Platzbecker,U. (2012) Severe pernicious anemia with distinct cytogenetic and flow cytometric aberrations mimicking myelodysplastic syndrome. *Ann. Hematol.*, **91**, 1979–1981.
 164. Chintagumpala,M.M., Dreyer,Z.A., Steuber,C.P. and Cooley,L.D. (1996) Pancytopenia with chromosomal fragility: vitamin B12 deficiency. *J. Pediatr. Hematol. Oncol.*, **18**, 166–170.
 165. Maltby,E.L. and Higgins,S. (1987) Folate sensitive site at 10q23 and its expression as a deletion. *J. Med. Genet.*, **24**, 299.
 166. Morel,C.F., Duncan,A.M.V. and Désilets,V. (2005) A fragile site at 10q23 (FRA10A) in a phenytoin-exposed fetus: A case report and review of the literature. *Prenat. Diagn.*, **25**, 318–321.
 167. De Leon-Luis,J., Santolaya-Forgas,J., May,G., Tonk,V., Shelton,D. and Galan,I. (2005) Prenatal diagnosis of FRA10A: a case report and literature review. *Am. J. Med. Genet. A*, **136**, 63–65.
 168. Ozisik,Y.Y., Meloni,A.M., Stone,J.F., Sandberg,A.A. and Surti,U. (1994) Spontaneous expression of the chromosome fragile site at 10q23 in leiomyoma. *Cancer Genet. Cytogenet.*, **74**, 73–75.
 169. Sarafidou,T., Kahl,C., Martinez-Garay,I., Mangelsdorf,M., Gesk,S., Baker,E., Kokkinaki,M., Talley,P., Maltby,E.L., French,L., et al. (2004) Folate-sensitive fragile site FRA10A is due to an expansion of a CGG repeat in a novel gene, FRA10AC1, encoding a nuclear protein. *Genomics*, **84**, 69–81.
 170. Sashindran,V.K., Aggarwal,V. and Khera,A. (2022) Prevalence of Vitamin B12 deficiency in elderly population (>60 years) presenting with dementia to outpatient department. *Med. J. Armed Forces India*, **78**, 94–98.
 171. Pinto,W.B.V.d.R., Souza,P.V.S.d., Rogério,R.M., Pedroso,J.L. and Barsottini,O.G.P. (2014) Vitamin B12 deficiency mimicking neuroimaging features of motor neuron disease. *Arg. Neuropsiquiatr.*, **72**, 85.
 172. Chen,A.T., Reidy,J.A., Annett,J.L., Welty,T.K. and Zhou,H.G. (1989) Increased chromosome fragility as a consequence of blood folate levels, smoking status, and coffee consumption. *Environ. Mol. Mutagen.*, **13**, 319–324.
 173. Barale,R., Chelotti,L., Davini,T., Del Ry,S., Andreassi,M.G., Ballardini,M., Bulleri,M., He,J., Baldacci,S., Di Pede,F., et al. (1998) Sister chromatid exchange and micronucleus frequency in human lymphocytes of 1,650 subjects in an Italian population: II. Contribution of sex, age, and lifestyle. *Environ. Mol. Mutagen.*, **31**, 228–242.
 174. Maffei,F., Fimognari,C., Castelli,E., Stefanini,G.F., Forti,G.C. and Hrelia,P. (2000) Increased cytogenetic damage detected by FISH analysis on micronuclei in peripheral lymphocytes from alcoholics. *Mutagenesis*, **15**, 517–523.
 175. Demirhan,O. and Tastemir,D. (2008) Cytogenetic effects of ethanol on chronic alcohol users. *Alcohol Alcohol.*, **43**, 127–136.
 176. Ueda,K., Sakai,C., Ishida,T., Morita,K., Kobayashi,Y., Horikoshi,Y., Baba,A., Okazaki,Y., Yoshizumi,M., Tashiro,S., et al. (2023) Cigarette smoke induces mitochondrial DNA damage and activates cGAS-STING pathway: application to a biomarker for atherosclerosis. *Clin. Sci. (Lond.)*, **137**, 163–180.
 177. Hesdorffer,C.S. and Longo,D.L. (2015) Drug-induced megaloblastic anemia. *N. Engl. J. Med.*, **373**, 1649–1658.
 178. Czuppa,M., Dhingra,A., Zhou,Q., Schludi,C., König,L., Scharf,E., Farny,D., Dalmia,A., Täger,J., Castillo-Lizardo,M., et al. (2022) Drug screen in iPSC-Neurons identifies nucleoside analogs as inhibitors of (G4C2)_n expression in C9orf72 ALS/FTD. *Cell Rep.*, **39**, 110913.
 179. Chiurazzi,P., Pomponi,M.G., Pietrobono,R., Bakker,C.E., Neri,G. and Oostra,B.A. (1999) Synergistic effect of histone hyperacetylation and DNA demethylation in the reactivation of the FMR1 gene. *Hum. Mol. Genet.*, **8**, 2317–2323.
 180. Lamparska,K., Clark,J., Babilonia,G., Bedell,V., Yip,W. and Smith,S.S. (2012) 2'-Deoxyriboguananylyrea, the primary breakdown product of 5-aza-2'-deoxyribocytidine, is a mutagen, an epimutagen, an inhibitor of DNA methyltransferases and an inducer of 5-azacytidine-type fragile sites. *Nucleic Acids Res.*, **40**, 9788–9801.
 181. Feichtinger,W. and Schmid,M. (1989) Increased frequencies of sister chromatid exchanges at common fragile sites (1)(q42) and (19)(q13). *Hum. Genet.*, **83**, 145–147.
 182. Rodríguez-Reyes,R. and Morales-Ramírez,P. (2011) The in vivo induction of sister chromatid exchange by the demethylating agent 5-aza-2'-deoxycytidine. *Mutagenesis*, **26**, 551–554.
 183. Haaf,T., Ott,G. and Schmid,M. (1986) Differential inhibition of sister chromatid condensation induced by 5-azadeoxycytidine in human chromosomes. *Chromosoma*, **94**, 389–394.
 184. Davidson,S., Crowther,P., Radley,J. and Woodcock,D. (1992) Cytotoxicity of 5-aza-2'-deoxycytidine in a mammalian cell system. *Eur. J. Cancer*, **28**, 362–368.
 185. Gijssels,I., Van Mossevelde,S., van der Zee,J., Sieben,A., Engelborghs,S., De Bleecker,J., Ivanou,A., Deryck,O., Edbauer,D., Zhang,M., et al. (2016) The C9orf72 repeat size correlates with onset age of disease, DNA methylation and transcriptional downregulation of the promoter. *Mol. Psychiatry*, **21**, 1112–1124.
 186. Kojak,N., Kuno,J., Fittipaldi,K.E., Khan,A., Wenger,D., Glasser,M., Donnianni,R.A., Tang,Y., Zhang,J., Huling,K., et al. (2024) Somatic and intergenerational G4C2 hexanucleotide repeat instability in a human C9orf72 knock-in mouse model. *Nucleic Acids Res.*, **52**, 5732–5755.
 187. Russ,J., Liu,E.Y., Wu,K., Neal,D., Suh,E., Irwin,D.J., McMillan,C.T., Harms,M.B., Cairns,N.J., Wood,E.M., et al. (2015) Hypermethylation of repeat expanded C9orf72 is a clinical and molecular disease modifier. *Acta Neuropathol.*, **129**, 39–52.

188. Zhang, M., Tartaglia, M.C., Moreno, D., Sato, C., McKeever, P., Weichert, A., Keith, J., Robertson, J., Zinman, L. and Rogaeva, E. (2017) DNA methylation age-acceleration is associated with disease duration and age at onset in C9orf72 patients. *Acta Neuropathol.*, **134**, 271–279.
189. Zhang, M., McKeever, P.M., Xi, Z., Moreno, D., Sato, C., Bergsma, T., McGoldrick, P., Keith, J., Robertson, J., Zinman, L., et al. (2020) DNA methylation age acceleration is associated with ALS age of onset and survival. *Acta Neuropathol.*, **139**, 943–946.
190. Galkin, F., Kovalchuk, O., Koldasbayeva, D., Zhavoronkov, A. and Bischof, E. (2023) Stress, diet, exercise: common environmental factors and their impact on epigenetic age. *Ageing Res. Rev.*, **88**, 101956.
191. Fitzgerald, K.N., Hodges, R., Hanes, D., Stack, E., Cheishvili, D., Szyf, M., Henkel, J., Twedt, M.W., Giannopoulou, D., Herdell, J., et al. (2021) Potential reversal of epigenetic age using a diet and lifestyle intervention: a pilot randomized clinical trial. *Ageing (Albany NY)*, **13**, 9419–9432.
192. Sae-Lee, C., Corsi, S., Barrow, T.M., Kuhnle, G.G.C., Bollati, V., Mathers, J.C. and Byun, H.-M. (2018) Dietary intervention modifies DNA methylation age assessed by the epigenetic clock. *Mol. Nutr. Food Res.*, **62**, e1800092.
193. Liu, Y., Huang, Z., Liu, H., Ji, Z., Arora, A., Cai, D., Wang, H., Liu, M., Simko, E.A.J., Zhang, Y., et al. (2023) DNA-initiated epigenetic cascades driven by C9orf72 hexanucleotide repeat. *Neuron*, **111**, 1205–1221.
194. Rapkin, L.M., Ahmed, K., Dulev, S., Li, R., Kimura, H., Ishov, A.M. and Bazett-Jones, D.P. (2015) The histone chaperone DAXX maintains the structural organization of heterochromatin domains. *Epigenetics Chromatin*, **8**, 44.
195. He, Q., Kim, H., Huang, R., Lu, W., Tang, M., Shi, F., Yang, D., Zhang, X., Huang, J., Liu, D., et al. (2015) The Daxx/Atrx complex protects tandem repetitive elements during DNA hypomethylation by promoting H3K9 trimethylation. *Cell Stem Cell*, **17**, 273–286.
196. Scott, W.A., Dhanji, E.Z., Dyakov, B.J.A., Dreseris, E.S., Asa, J.S., Grange, L.J., Mirceta, M., Pearson, C.E., Stewart, G.S., Gingras, A.-C., et al. (2021) ATRX proximal protein associations boast roles beyond histone deposition. *PLoS Genet.*, **17**, e1009909.
197. van Blitterswijk, M., Mullen, B., Nicholson, A.M., Bieniek, K.F., Heckman, M.G., Baker, M.C., DeJesus-Hernandez, M., Finch, N.A., Brown, P.H., Murray, M.E., et al. (2014) TMEM106B protects C9ORF72 expansion carriers against frontotemporal dementia. *Acta Neuropathol.*, **127**, 397–406.
198. van Blitterswijk, M., Mullen, B., Heckman, M.G., Baker, M.C., DeJesus-Hernandez, M., Brown, P.H., Murray, M.E., Hsiung, G.-Y.R., Stewart, H., Karydas, A.M., et al. (2014) Ataxin-2 as potential disease modifier in C9ORF72 expansion carriers. *Neurobiol. Aging*, **35**, 2421.
199. van Blitterswijk, M., Mullen, B., Wojtas, A., Heckman, M.G., Diehl, N.N., Baker, M.C., DeJesus-Hernandez, M., Brown, P.H., Murray, M.E., Hsiung, G.-Y.R., et al. (2014) Genetic modifiers in carriers of repeat expansions in the C9ORF72 gene. *Mol. Neurodegener.*, **9**, 38.
200. Pliner, H.A., Mann, D.M. and Traynor, B.J. (2014) Searching for Grendel: origin and global spread of the C9ORF72 repeat expansion. *Acta Neuropathol.*, **127**, 391–396.
201. Biasiotto, G. and Zanella, I. (2019) The effect of C9orf72 intermediate repeat expansions in neurodegenerative and autoimmune diseases. *Mult. Scler. Relat. Disord.*, **27**, 42–43.
202. Burberry, A., Suzuki, N., Wang, J.-Y., Moccia, R., Mordes, D.A., Stewart, M.H., Suzuki-Uematsu, S., Ghosh, S., Singh, A., Merkle, F.T., et al. (2016) Loss-of-function mutations in the C9ORF72 mouse ortholog cause fatal autoimmune disease. *Sci. Transl. Med.*, **8**, 347ra93.
203. B eland, L.-C., Markovinic, A., Jakovac, H., De Marchi, F., Bilic, E., Mazzini, L., Kriz, J. and Munitic, I. (2020) Immunity in amyotrophic lateral sclerosis: blurred lines between excessive inflammation and inefficient immune responses. *Brain Commun.*, **2**, fcaa124.
204. Burberry, A., Wells, M.F., Limone, F., Couto, A., Smith, K.S., Keaney, J., Gillet, G., van Gestel, N., Wang, J.-Y., Pietilainen, O., et al. (2020) C9orf72 suppresses systemic and neural inflammation induced by gut bacteria. *Nature*, **582**, 89–94.
205. Bertrand, A., Wen, J., Rinaldi, D., Houot, M., Sayah, S., Camuzat, A., Fournier, C., Fontanella, S., Routier, A., Couratier, P., et al. (2018) Early cognitive, structural, and microstructural changes in presymptomatic C9orf72 carriers younger than 40 years. *JAMA Neurol.*, **75**, 236–245.
206. Querin, G., Bede, P., El Mendil, M.M., Li, M., P el egrini-Issac, M., Rinaldi, D., Catala, M., Saracino, D., Salachas, F., Camuzat, A., et al. (2019) Presymptomatic spinal cord pathology in c9orf72 mutation carriers: a longitudinal neuroimaging study. *Ann. Neurol.*, **86**, 158–167.
207. Burgess, R.C., Burman, B., Kruhlak, M.J. and Misteli, T. (2014) Activation of DNA damage response signaling by condensed chromatin. *Cell Rep.*, **9**, 1703–1717.
208. Jacome, A. and Fernandez-Capetillo, O. (2011) Lac operator repeats generate a traceable fragile site in mammalian cells. *EMBO Rep.*, **12**, 1032–1038.
209. Soutoglou, E., Dorn, J.F., Sengupta, K., Jasin, M., Nussenzweig, A., Ried, T., Danuser, G. and Misteli, T. (2007) Positional stability of single double-strand breaks in mammalian cells. *Nat. Cell Biol.*, **9**, 675–682.
210. Soutoglou, E. and Misteli, T. (2008) Activation of the cellular DNA damage response in the absence of DNA lesions. *Science*, **320**, 1507–1510.
211. Freaney, J.E., Zhang, Q., Yigit, E., Kim, R., Widom, J., Wang, J.-P. and Horvath, C.M. (2014) High-density nucleosome occupancy map of human chromosome 9p21–22 reveals chromatin organization of the type I interferon gene cluster. *J. Interferon Cytokine Res.*, **34**, 676–685.
212. Apostolou, E. and Thanos, D. (2008) Virus infection induces NF-kappaB-dependent interchromosomal associations mediating monoallelic IFN-beta gene expression. *Cell*, **134**, 85–96.
213. Pang, W. and Hu, F. (2021) Cellular and physiological functions of C9ORF72 and implications for ALS/FTD. *J. Neurochem.*, **157**, 334–350.
214. Quinodoz, S.A., Ollikainen, N., Tabak, B., Palla, A., Schmidt, J.M., Detmar, E., Lai, M.M., Shishkin, A.A., Bhat, P., Takei, Y., et al. (2018) Higher-order inter-chromosomal hubs shape 3D genome organization in the nucleus. *Cell*, **174**, 744–757.
215. Jagannathan, M. and Yamashita, Y.M. (2017) Function of junk: pericentromeric satellite DNA in chromosome maintenance. *Cold Spring Harb. Symp. Quant. Biol.*, **82**, 319–327.
216. Jagannathan, M., Cummings, R. and Yamashita, Y.M. (2018) A conserved function for pericentromeric satellite DNA. *Elife*, **7**, e34122.
217. Malachowski, T., Chandradoss, K.R., Boya, R., Zhou, L., Cook, A.L., Su, C., Pham, K., Haws, S.A., Kim, J.H., Ryu, H.-S., et al. (2023) Spatially coordinated heterochromatinization of long synaptic genes in fragile X syndrome. *Cell*, **186**, 5840–5858.
218. Droppelmann, C.A., Campos-Melo, D., Moszczynski, A.J., Amzil, H. and Strong, M.J. (2019) TDP-43 aggregation inside micronuclei reveals a potential mechanism for protein inclusion formation in ALS. *Sci. Rep.*, **9**, 19928.
219. Fritsch, L.E., Ju, J., Gudenschwager Basso, E.K., Soliman, E., Paul, S., Chen, J., Kaloss, A.M., Kowalski, E.A., Tuhy, T.C., Somaia, R.D., et al. (2022) Type I interferon response is mediated by NLRX1-cGAS-STING signaling in brain injury. *Front. Mol. Neurosci.*, **15**, 852243.
220. Song, X., Ma, F. and Herrup, K. (2019) Accumulation of cytoplasmic DNA due to ATM deficiency activates the microglial viral response system with neurotoxic consequences. *J. Neurosci.*, **39**, 6378–6394.

221. Quek,H., Luff,J., Cheung,K., Kozlov,S., Gatei,M., Lee,C.S., Bellingham,M.C., Noakes,P.G., Lim,Y.C., Barnett,N.L., *et al.* (2017) Rats with a missense mutation in *Atm* display neuroinflammation and neurodegeneration subsequent to accumulation of cytosolic DNA following unrepaired DNA damage. *J. Leukoc. Biol.*, **101**, 927–947.
222. Lupski,J.R. (2023) Somatic cell structural variant mutagenesis and neurologic disease. *Cell Genom.*, **3**, 100376.
223. Schuy,J., Grochowski,C.M., Carvalho,C.M.B. and Lindstrand,A. (2022) Complex genomic rearrangements: an underestimated cause of rare diseases. *Trends Genet.*, **38**, 1134–1146.
224. Campbell,I.M., Shaw,C.A., Stankiewicz,P. and Lupski,J.R. (2015) Somatic mosaicism: implications for disease and transmission genetics. *Trends Genet.*, **31**, 382–392.
225. Coffee,B., Ikeda,M., Budimirovic,D.B., Hjelm,L.N., Kaufmann,W.E. and Warren,S.T. (2008) Mosaic FMR1 deletion causes fragile X syndrome and can lead to molecular misdiagnosis: a case report and review of the literature. *Am. J. Med. Genet. A*, **146A**, 1358–1367.
226. Gómez-Rodríguez,M.J., Morales-Conejo,M., Arteché-López,A., Sánchez-Calvín,M.T., Quesada-Espinosa,J.F., Gómez-Manjón,I., Palma-Milla,C., Lezana-Rosales,J.M., Pérez de la Fuente,R., Martín-Ramos,M.-L., *et al.* (2022) Fragile X syndrome caused by maternal somatic mosaicism of FMR1 gene: case report and literature review. *Genes (Basel)*, **13**, 1609.
227. Gonçalves,T.F., dos Santos,J.M., Gonçalves,A.P., Tassone,F., Mendoza-Morales,G., Ribeiro,M.G., Kahn,E., Boy,R., Pimentel,M.M.G. and Santos-Rebouças,C.B. (2016) Finding FMR1 mosaicism in Fragile X syndrome. *Expert Rev. Mol. Diagn.*, **16**, 501–507.
228. Hensel,C.H., Vanzo,R.J., Martin,M.M., Ling,L., Aliaga,S.M., Bui,M., Francis,D.I., Twede,H., Field,M.H., Morison,J.W., *et al.* (2019) Abnormally methylated FMR1 in absence of a detectable full mutation in a U.S.A patient cohort referred for fragile X testing. *Sci. Rep.*, **9**, 15315.
229. Prawer,Y., Hunter,M., Cronin,S., Ling,L., Aliaga Vera,S., Fahey,M., Gelfand,N., Oertel,R., Bartlett,E., Francis,D., *et al.* (2018) Prenatal diagnosis of fragile X syndrome in a twin pregnancy complicated by a complete retraction. *Genes (Basel)*, **9**, 287.
230. Pandelache,A., Francis,D., Oertel,R., Dickson,R., Sachdev,R., Ling,L., Gamage,D. and Godler,D.E. (2021) Detection of cryptic fragile X full mutation alleles by southern blot in a female and her foetal DNA via chorionic villus sampling, complicated by mosaicism for 45,X0/46,XX/47,XXX. *Genes (Basel)*, **12**, 798.
231. Mätlik,K., Baffuto,M., Kus,L., Deshmukh,A.L., Davis,D.A., Paul,M.R., Carroll,T.S., Caron,M.-C., Masson,J.-Y., Pearson,C.E., *et al.* (2024) Cell type specific CAG repeat expansions and toxicity of mutant Huntingtin in human striatum and cerebellum. *Nat. Genet.*, **56**, 383–394.
232. Pressl,C., Mätlik,K., Kus,L., Darnell,P., Luo,J.-D., Paul,M.R., Weiss,A.R., Liguore,W., Carroll,T.S., Davis,D.A., *et al.* (2023) Selective vulnerability of layer 5a corticostriatal neurons in Huntington's disease. *Neuron*, **112**, 924–941.
233. Ziff,O.J., Neeves,J., Mitchell,J., Tyzack,G., Martinez-Ruiz,C., Luisier,R., Chakrabarti,A.M., McGranahan,N., Litchfield,K., Boulton,S.J., *et al.* (2023) Integrated transcriptome landscape of ALS identifies genome instability linked to TDP-43 pathology. *Nature Commun.*, **14**, 2176.
234. Albert,S.M. (2010) Neurodegenerative disease and cancer: a critical role for melanoma? *Neuroepidemiology*, **35**, 305–306.
235. Baade,P.D., Herrero Hernández,E., Freedman,D.M., Smithers,B.M. and Fritschi,L. (2010) No role for melanoma treatment in the association between melanoma and amyotrophic lateral sclerosis or Parkinson's disease. *Neuroepidemiology*, **35**, 303–304.
236. Baade,P.D., Fritschi,L. and Freedman,D.M. (2007) Mortality due to amyotrophic lateral sclerosis and Parkinson's disease among melanoma patients. *Neuroepidemiology*, **28**, 16–20.
237. Freedman,D.M., Curtis,R.E., Daugherty,S.E., Goedert,J.J., Kuncel,R.W. and Tucker,M.A. (2013) The association between cancer and amyotrophic lateral sclerosis. *Cancer Causes Control.*, **24**, 55–60.
238. Freedman,D.M., Travis,L.B., Gridley,G. and Kuncel,R.W. (2005) Amyotrophic lateral sclerosis mortality in 1.9 million US cancer survivors. *Neuroepidemiology*, **25**, 176–180.